

# Full-scale observations of dynamic and static axial responses of offshore piles driven in chalk and tills

Buckley, R.M.<sup>1</sup>, roisin.buckley@eng.ox.ac.uk

Jardine, R.J.<sup>2</sup>,

Kontoe, S.<sup>2</sup>,

Barbosa, P.<sup>3</sup>

Schroeder, F.C.<sup>4</sup>

1. Department of Engineering Science, Oxford University, formerly Department of Civil & Environmental Engineering, Imperial College London 2. Department of Civil & Environmental Engineering, Imperial College London, UK 3. Iberdrola Renovables Offshore, Deutschland, Berlin, Germany 4. Geotechnical Consulting Group LLP, London, UK

(MAIN TEXT 8198 WORDS)

## ABSTRACT

---

This paper describes and interprets tests on piles driven through glacial tills and chalk at a Baltic Sea windfarm, covering an advance trial campaign and later production piling. The trials involved six instrumented 1.37m diameter steel open-ended tubes driven in water depths up to 42m. Three piles were tested statically, with dynamic re-strike tests on paired piles, at 12-15 week ages. Instrumented dynamic driving and re-strike monitoring followed on up to 3.7m diameter production piles. During driving, the shaft resistances developed at fixed depths below sea-bed fell markedly during driving, with particularly sharp reductions occurring in the chalk. Shaft resistances increased markedly after driving and good agreement was seen between long-term capacities interpreted from parallel static and dynamic tests. Analyses employing the sites' geotechnical profiles show long-term shaft resistances in the chalk that far exceed those indicated by current design recommendations, while newly proposed procedures offer good predictions. The shaft capacities mobilised in the low-plasticity tills also grew significantly over time, within the broad ranges reported for sandy soils. The value of offshore field testing in improving project outcomes and design rules is demonstrated; the approach described may be applied to other difficult seabed conditions.

*Keywords:* chalk, piles & piling, full-scale tests, glacial soils

## 1 INTRODUCTION

---

2 Most offshore oil, gas and wind-turbine structures rely on open-ended driven steel piles, whose outside  
3 diameters,  $D$ , range between 0.8 and 8m and penetrations may exceed 100m ([Hamre, 2018](#), [Jardine,](#)  
4 [2019](#)). Open-piles are also driven for bridge, harbour and other foundations. Field testing is required to  
5 verify load carrying capacities under some regulatory regimes, as in the German ([BSH, 2015](#))  
6 framework, where EC7 applies in accordance with [DIN \(2009, 2012\)](#). While static load tests are  
7 common onshore, they are usually deemed unfeasible offshore. Checks may be conducted at analogous  
8 onshore sites (e.g. [Al-Shafei et al., 1994](#), [Lahrs and Kallias, 2013](#)) and through dynamic driving  
9 monitoring offshore. However, it is often difficult to match field conditions onshore, or interpret  
10 dynamic tests accurately. Onshore tests show axial capacities increasing significantly with time after  
11 driving in sands ([Jardine et al., 2006](#)), low-plasticity clays ([Karlsrud et al., 2014](#)) and in chalk  
12 formations, for which accurate capacity predictions are particularly hard to make ([see Lord et al., 2002,](#)  
13 [Ciavaglia et al., 2017](#), or [Buckley et al., 2018a](#)). However, long-term re-strike check-tests are rarely  
14 undertaken offshore.

15 This paper describes and interprets novel static and dynamic testing for the Wiking windfarm, which  
16 is located roughly midway between the Rugen and Bornholm islands in the German Baltic. Seventy  
17 5MW Wind-Turbine Generators (WTGs) and an Offshore Substation (OSS) were installed in 2017.  
18 Each WTG's jacket structure is founded on four 2.7m outside diameter,  $D$ , tubular driven steel piles,  
19 while the OSS relies on six 3.7m diameter piles. The piles, whose environmental loads invoke axial  
20 'push-pull' and lateral pile reactions, penetrate through dense/stiff sandy tills over low-medium density  
21 chalk and in some cases, limestone ([Barbosa et al., 2015a](#), [Barbosa et al., 2015b](#)).

22 Iberdrola, the project developers, conducted comprehensive site investigation and 'pre-construction'  
23 piling campaigns at Wiking. Six instrumented 1.37m diameter steel (Grade S355) open-ended piles  
24 were driven with dynamic monitoring, in up to 42m of water, near the WK38, WK43 and WK70 turbine  
25 locations. One pile was tested statically at each location after 12-15 weeks of ageing, with novel,  
26 remotely-operated seabed testing systems, before conducting parallel dynamic re-strikes on adjacent

paired piles. Figure 1 sets out the relative positions of the piles, boreholes and piezocone/CPT tests at each location. Additional instrumented dynamic driving and re-strike monitoring followed at five ‘production’ piling locations, as summarised in Table 1. A joint project involving Innovate-UK, Iberdrola, Imperial College and Geotechnical Consulting Group (GCG) supported the offshore research with parallel onshore pile experiments, laboratory studies and analytical developments.

## BACKGROUND

---

Pile shaft capacities,  $Q_s$  represent the integration over their perimeters  $\pi D$  (where  $D$  is diameter) and shaft lengths,  $L_p$ , of the contributions made by local limiting shaft shear stresses,  $\tau_f$ , which usually vary with depth:

$$Q_s = \pi D \int_0^{L_p} \tau_f dz \quad \text{Eq. 1}$$

Offshore pile designers often employ the American Petroleum Institute (API) RP2 GEO (API, 2014) or ISO 19902:2007 (ISO, 2007) recommendations in sand layers to predict  $\tau_f$  from the estimated in situ effective overburden pressure,  $\sigma'_{vo}$ , through  $\beta$  coefficients, or from the local CPT tip resistances  $q_c$ , choosing between four ‘CPT’ procedures cited in the commentary. The latter include the ICP-05 procedure described by Jardine *et al.* (2005) in which  $\tau_f$  is related to local shaft radial effective stresses at failure,  $\sigma'_{rf}$  by the Coulomb expression given as Eq. 2:

$$\tau_f = \sigma'_{rf} \tan \delta' \quad \text{Eq. 2}$$

The radial effective stresses reduce with increasing  $h/R^*$  where  $h$  is the relative distance from the pile tip and  $R^*$  is the pile’s equivalent ‘solid’ radius,  $R^* = (R^2 - R_i^2)^{0.5}$  where  $R_i$  and  $R$  are the inner and outer radii. Interface shear angles,  $\delta'$  can vary from peak,  $\delta'_{peak}$  to ultimate,  $\delta'_{ult}$  values when local slip occurs in brittle soils. However, shaft capacities can grow markedly in sand layers over the weeks and months that follow driving and exceed the medium-term (typically ten to thirty-day age) estimates provided by approaches such as the ICP-05; Jardine *et al.* (2006).

Offshore designers usually base their shaft capacity assessments for clay layers on the local undrained shear strengths,  $s_u$  and  $\alpha$  coefficients that vary with  $s_u/\sigma'_{vo}$ . Other methods exist to assess shaft capacity in clay e.g. the “Fugro-96” method; [Kolk and der Velde \(1996\)](#), the “NGI=05” method; [Karlsrud et al. \(2005\)](#) and the ICP-05 clay method set out by [Jardine et al. \(2005\)](#), which also employs Eq. 2 and recognises, as with clays, a dependence of  $\sigma'_{rf}$  on  $h/R^*$ . [Lehane et al. \(2013\)](#) have also proposed direct use of CPT cone resistance,  $q_t$  for clays and report encouraging results for their “UWA-13” methods in comparison with outcomes from 43 static load tests. Significant effects of pile age after driving on shaft capacity have also been noted in low plasticity clays; [Karlsrud et al. \(2014\)](#).

[Lehane et al. \(2017\)](#) carefully quality-assured database included only one site (Cowden in Humberside, UK) where stiff low plasticity glacial tills contributed the main parts of the piles’ shaft capacities. More high-quality tests are needed to assess how routine design methods apply to such strata. [Weltman and Healy \(1978\)](#) presented a review for UK glacial clay tills and concluded that, for the tests they analysed, the driven piles’  $\alpha$  coefficients declined, as often expected, with increasing  $s_u$  to reach 0.4 at the maximum  $s_u$  ( $\approx 210$  kPa) considered. Well-graded offshore tills with significant fines contents are sometimes treated as clays, especially when they manifest non-hydrostatic trends in piezocone tests. However, low-plasticity sandy offshore tills, such as those encountered at Wikingen, may not behave in the same ways as terrestrial tills, marine or alluvial clays.

The most common current industrial practice is to apply CIRIA C574 to open-piles driven in chalk. A conservative interpretation by [Lord et al. \(2002\)](#) of six static tests led to CIRIA C574 recommending fixed ultimate unit shaft resistances of 20 and 120kPa for low-medium and high density cases respectively. Noting the paucity of chalk cases, the Authors conducted multiple experiments with driven steel open-ended piles and jacked highly instrumented Imperial College Piles (ICP) in low-medium density chalk at St. Nicholas-at-Wade in Kent, UK. [Buckley et al. \(2018a\)](#) and [Buckley et al. \(2018b\)](#) concluded that:

1. Very high excess pore water pressures develop around pile tips and low strength chalk putty annuli form around their shafts during driving;

2. Chalk's relatively high in-situ permeability allows partial drainage during both CPT penetration and pile installation. Marked water content reductions develop as pore-pressures dissipate;
3. Low average shaft resistances, broadly comparable with CIRIA C574, apply during and immediately after driving. However, shaft shear stress distributions vary markedly with depth and show far stronger reductions with relative pile tip depth  $h/R^*$  than apply in clays or sands;
4. The shaft radial effective stresses developed during installation correlate with the CPT cone resistance, mobilising comparably low  $\sigma'_{rf}/q_t$  ratios to crushable calcareous sands;
5. Driven open-ended piles' shaft capacities can increase five-fold after driving to give long-term unit shaft resistances far above the CIRIA C574 values. Set-up rates are sensitive to site specific features such as the discontinuity sets, the installation process and physio-chemical processes;
6. Eq. 2 describes shaft failure accurately in chalks, with  $\delta'$  angles that match laboratory interface tests. As in sands, shaft radial effective stresses increase during static loading to failure.

The above results derived principally from relatively small-scale experiments conducted at an onshore site. This paper reports full-scale static and dynamic tests that explore the corresponding behaviours of large piles driven for the Wikingen offshore windfarm project. The Wikingen ground conditions are considered first, setting out the geotechnical parameters required for test analysis. The pile testing programme and procedures are then outlined before reporting and interpreting the outcomes. Finally, the offshore data are employed to assess the applicability of recently proposed design rules for piles driven in chalk.

## GROUND CONDITIONS

---

The Wikingen stratigraphy consists of Pleistocene glacial and fluvoglacial tills over low-medium density structured Upper-to-Late Cretaceous chalk, which is incised by narrow sub-glacial channels infilled with tills; Upper Cretaceous or Danian limestone is also encountered. The windfarm area is large and representative pile test locations were chosen that cover the most adverse conditions ([CIJV, 2014b](#)) and encompass the ground profiles and pile penetrations,  $L_p$ , summarised in Table 1. The WK13 and WK38 test piles were dominated by glacial till, while the WK08 and WK42 production piles

penetrated both glacial and fluvioglacial tills. The OSS, WK43 and WK70 piles are dominated by low-medium density chalk, while WK11 penetrated almost equal proportions of glacial till and chalk.

### *In-situ testing*

As indicated in Figure 1, at least one borehole and CPT were undertaken at each test location. As might be expected, conditions are highly variable within the low plasticity glacial and fluvioglacial strata. [Augustesen et al. \(2015\)](#) and [Barbosa et al. \(2017\)](#) treated the glacial till and fluvioglacial till layers as clays in their initial design studies. Secant shear stiffnesses were measured in the glacial till by high pressure dilatometer tests ([Cambridge-Insitu, 2013](#)), while shear,  $V_s$ , and compression wave,  $V_p$ , velocities were logged in the chalk through P-S probes suspended in boreholes ([CIJV, 2013](#)). Figure 2 shows profiles of maximum shear modulus,  $G_{vh}$  in the chalk, as calculated from  $V_s$  measurements at five locations. Consistent with nearby observations by [Obst et al. \(2017\)](#),  $V_s$  typically ranged from 0.8 to 1.1km/s, increasing only slightly with depth. The  $G_{max}$  shear moduli were assessed by [CIJV \(2014a\)](#) as varying linearly with depth below seabed ( $z$ , in m) in the low-medium density chalk:

$$G_{max} = 17.3z + 895 \text{ (MPa)}$$

Eq. 3

The corresponding  $V_p$  velocities were all  $\approx 2$ km/s.

Figure 3 shows  $q_t$  profiles assessed at the three static test sites, as well as the WK42 production location where fluvioglacial till is present. The glacial tills generally showed  $3 < q_t < 30$ MPa, with peaks up to 50MPa in isolated thin dense sand layers and sleeve frictions,  $100 < f_s < 300$ kPa. Excess penetration pore pressures, measured at the  $u_2$  position, showed generally negative values (-100 to -250kPa) with discrete peaks up to +1MPa. The relatively deep fluvioglacial till encountered at WK42 showed lower average  $q_t$  values (generally  $< 10$ MPa), an  $f_s$  range of 300 to 600kPa and positive penetration  $u_2$  values up to 1MPa, all suggesting higher fines contents than in the glacial till. Figure 4 plots the soil behaviour type index,  $I_c$  ([Robertson, 1990](#)) in the glacial/fluvioglacial till layers. This re-analysis classifies the glacial tills as silty sands and sandy silts, while the fluvioglacial tills appear as sandy silts to silty clays. Considering the glacial till's  $q_t$  range of 6-20MPa, [Baldi et al. \(1989\)](#)'s correlation for sandy soils suggests maximum shear moduli in the 200-1500MPa range.

Most of the Wikinger chalk classifies as structured low-medium density with Grade A1/A2 ([Bowden et al., 2002](#)). It is extremely weak with closely spaced, closed or clean fractures. The chalk  $q_t$  profiles were averaged over 0.3m penetration intervals, following [Smith \(2001\)](#), generally giving 10 to 20MPa in the structured chalk, but with isolated peaks up to 60MPa. Sleeve frictions generally fell between 200 and 400kPa, while  $u_2$  values were remarkably high and increased to reach 10MPa at 30m below seabed. Field permeability is often sufficiently high in intact chalk for it to drain freely under field foundation loading conditions ([Lord et al., 2002](#)). Piezocone dissipation tests performed at St Nicholas-at-Wade in a similar low-medium density fractured Grade B2/B3 chalk indicated times for 50% dissipation of penetration generated excess pore water pressures of less than 10 seconds; [Buckley et al. \(2018a\)](#).

Fully continuous chalk CPT profiles were available for only four test sites and some profiles terminated after shallow penetrations into the chalk (Table 1). As noted earlier, correlations have been proposed for various geo-materials between CPT  $q_t$  and  $G_{max}$  or  $V_s$  (see for example [Baldi et al. \(1989\)](#), [Mayne and Rix \(1993\)](#) or [McGann et al. \(2015\)](#)). A local relationship of this type was established for the Wikinger chalk. The  $q_t$  -  $V_s$  data pairs presented in Figure 5, which exclude peaks associated with flints and the Danian limestone, indicate that the near-linear relationship given by Eq. 4 applies over the 9.5 to 63m depth range considered:

$$q_t = 21V_s^{1.1} \quad \text{Eq. 4}$$

$V_s$  is in km/s and  $q_t$  is in MPa. Eq. 4, which may not apply to different chalk sites, grades or densities, led to an average ratio for the calculated-to-measured  $q_t$  values of 1.01 and standard deviation of 0.16 at Wikinger. Although the  $q_t$  profiles adopted were averaged following the approach described by [Smith \(2001\)](#), some scatter is inevitable due to the significant  $q_t$  peaks associated with locally denser or more cemented layers and/or the presence of flints, which may not be recognised in the shear wave measurements. Eq. 4 was used to estimate  $q_t$  when  $V_s$  but not CPT data was available. Mean  $q_t$  trends from locations with similar ground profiles were adopted when  $V_s$  data was also absent.

## Laboratory testing

Index, anisotropically consolidated undrained (CAU) triaxial, oedometer and interface shear laboratory tests were conducted by GEO, Gardline Geosciences Ltd ([CIJV, 2013](#)) and [Fugro \(2013\)](#). Supplementary testing at Imperial College examined the interface shear behaviour of the glacial till ([Buckley, 2018](#)) and the time-dependent behaviour of the remoulded “putty” chalk that forms around pile shafts during driving ([Doughty et al., 2018](#)). Table 2 summarises the index properties of the three main strata; three key additional points are:

1. Figure 6 identifies the low plasticity glacial till as silty/clayey sand, with just over 10% clay on average, confirming the interpretation made using  $I_c$  shown on Figure 4. The fluvioglacial layers manifest higher fines fractions and 15 to 28% clay contents. Five out of eight oedometer tests on glacial till samples gave permeabilities (under in-situ stresses)  $\approx 10^{-7} \text{ m}^2/\text{s}$ , while the remaining three showed  $\approx 10^{-6} \text{ m}^2/\text{s}$ . These intermediate values fall below the range expected for clean sands and yet significantly above those for clay dominated tills. The fluvioglacial till's permeability values were generally lower, with five tests indicating less than  $10^{-7} \text{ m}^2/\text{s}$  and just one higher value.
2. The chalk classifies as structured low-medium density ( $\text{IDD} < 1.5 \text{ Mg/m}^3$ ) Grade A1/A2 ([Bowden et al., 2002](#)). Its Unconfined Compressive (UCS) Strengths ranged from 0.2-0.8MPa, falling below the 1.1 to 5MPa range proposed for low-medium density chalk by [Matthews and Clayton \(1993\)](#);
3. Either high density chalk or Danian limestone (with intact dry density,  $\text{IDD}$  up to  $\approx 1.9 \text{ Mg/m}^3$ ) was encountered between approximately 7.5m and 14m depth at the WK70 location.

The CAU triaxial tests presented in Appendix 1 illustrate the strongly dilative behaviour manifested by till samples when sheared undrained towards stable critical states, mobilising large axial strains and high final  $s_u$  values that would signify high Yield Stress Ratios (YSR) in clay strata; YSR often tends to infinity at shallow depths and ratios are limited here to 150. Location-specific  $s_u$  profiles were generated for axial capacity calculations (Figure 4), treating both tills as clays by applying an  $N_{kt}$  value of 22.5, which was found by site-specific correlation between CPT, CAU and Unconsolidated



Undrained (UU) triaxial tests. The interpretation led to remarkably high and non-uniform  $s_u$  values. The resulting  $s_u/\sigma'_{v0}$  ratios were employed as described in Appendix 2 to generate illustrative YSR profiles, which are also plotted in Figure 4. Appendix 2 also presents the interface ring shear tests performed on glacial (but unfortunately not fluvio-glacial) till samples, which gave  $\delta'_{ult}$  of 26.5-28°. Stiff, high YSR, low plasticity clay tills are generally insensitive ([Lehane \(1992\)](#), [Long and Menkiti \(2007\)](#) or [Ushev \(2018\)](#)) and sensitivity,  $S_t$  was assumed as unity for the Wikingier tills. [Buckley \(2018\)](#) gives further details of the till's compressibility, shear stiffness and critical state parameters.

Turning to the chalk, Appendix 1 reports CAU tests that showed high stiffness up to the onset (at notably small strains) of dilation followed by markedly brittle failure, confirming behaviour noted by ([e.g. Jardine et al., 1985](#)) and others. The peak shear strengths of low-density samples were consistent with  $\phi'=36^\circ$  and  $c'=150\text{kPa}$ , which may reflect cementing. A higher  $\phi'=36.4^\circ$  with  $c'\approx 200\text{kPa}$  applied to denser samples and these parameters are compatible with the lower end of the ranges for  $c'$  of 100kPa to >2MPa and  $\phi'$  of 36-42° quoted for intact chalk by [Lord et al. \(2002\)](#). [Doughty et al. \(2018\)](#) showed that intact Wikingier chalk, whose natural water contents usually lie close to their liquid limit, degrades readily to putty with  $s_u\approx 4\text{kPa}$  under compaction at constant water content. Fall cone tests showed mildly thixotropic behaviour after puttification, with modest increases in  $s_u$  developing through ageing. Far greater increases in  $s_u$  and stiffness could be obtained by consolidating the putty to higher effective stresses. Undrained triaxial tests on such consolidated puttified material indicated  $c'=0$  and  $M_{tc}=1.24$  ( $\phi'_{cv}\approx 31^\circ$ ), consistent with [Clayton \(1978\)](#) and [Razoaki \(2000\)](#). Interface ring-shear tests demonstrated  $\delta'_{ult}$  angles of 32-34° in the chalk ([Fugro, 2013](#)) similar to those reported by [Le et al. \(2014\)](#) and [Ziogos et al. \(2017\)](#) at comparable normal effective stress levels. Ring shear interface tests by [Chan et al. \(2019\)](#) gave comparable  $\delta'_{ult}$  values for chalk that increased only moderately with normal stress, up to the 400 kPa maximum investigated. [Ziogos et al. \(2017\)](#) reported marked reductions in  $\delta$  under much higher normal stresses. A single value of 33° was adopted in the analyses that follow. [Doughty \(2016\)](#) gives further details of the remoulded chalk's compressibility, shear stiffness and critical state parameters.

## PROGRAMME OF STATIC AND DYNAMIC PILE TESTS

---

### *Programme*

The two phases of pile testing at Wikingen are summarised in Table 3, which also identifies the individual tests' codes. The 'pre-construction' trial campaign involved six 1.37m diameter piles, driven in pairs at the WK38, WK43 and WK70 locations with dual sets of accelerometers and strain gauges attached near the pile heads. One pile from each pair was tested statically, 12-15 weeks after driving, shortly before an instrumented re-strike on the adjacent twin pile. The ageing periods were chosen to match the minimum durations anticipated between driving and turbine installation. Coupled cylindrical cavity expansion analyses ([Randolph and Wroth, 1979](#)) indicate that pore-pressure dissipation rates after driving are governed by non-dimensional time factors  $T = t c_v / (R^*)^2$ . It is difficult to ascribe field  $c_v$  values accurately for pile equalisation in clays ([Lehane et al., 2017](#)). However, piezometers mounted on open-ended, 762mm diameter, piles (with  $R^* = 0.17\text{m}$ ) driven in relatively low plasticity, high YSR, Lowestoft tills at Tilbrook Grange showed around 90% dissipation after 130 days ([Clarke et al., 1993](#)), while 2m diameter open steel piles (with  $R^* = 0.27\text{m}$ ) driven for the PISA programme in low plasticity Cowden till showed more than 90% dissipation after 100 days; [PISA \(2015\)](#). Noting that the 1.37m diameter, 40mm thick, Wikingen test piles have  $R^* = 0.23\text{m}$  and that the Wikingen tills' permeabilities (and operational  $c_v$  values) are significantly higher than those at Cowden or Tilbrook Grange, full dissipation was probably achieved before the static trial pile tests. Faster equalisation is expected in the far stiffer and more permeable chalk.

The second phase of testing included instrumented dynamic driving and re-strike monitoring at five production locations on six (up to 3.7m diameter) piles.

### *Pile and driving details*

The trial pile driving employed a Menck MHU 800S hydraulic hammer. Paired test piles were set  $\approx 8\text{m}$  apart, as shown in Figure 1, along with a third (un-instrumented) reaction pile. Self-weight penetrations of 2.6m were noted at WK38, where the soft Holocene cover was relatively thick, and less than 0.4m at WK43 and WK70 where the cover was thinner. The 2.7m diameter WTG and 3.7m diameter OSS

production piles were driven with a heavier Menck MHU 1200S. Penetrations of generally 15-25mm per blow were recorded in the till and 25-50mm per blow in the chalk during the pre-construction pile installations. The production piles showed less variable (10-20mm per blow) penetrations in both strata. All piles cored fully during installation, with their plugs rising above the seabed. Five to 42-minute driving pauses occurred for a variety of operational reasons.

#### *Dynamic analysis of driving*

Back analysis of the driving signals with IMPACT ([Randolph, 2008](#)) allowed assessments of the overall ‘equivalent static’ capacities and shaft load distributions developed during penetration and at the End of Driving (EOD), as well as in re-strike tests.

Annular piles displace much lower volumes of soil and develop lower (base and shaft) resistances than closed-ended piles (e.g. [Randolph, 2003](#), [Xu et al., 2006](#), [Gavin and Lehane, 2007](#)). [Chow \(1997\)](#) and [Jardine et al. \(2005\)](#) employed instrumented pile and pile plug resistance tests to show that internal shaft resistance reduces dramatically with increasing pile internal diameter and is likely to be both relatively minor and concentrated towards the bases of large diameter piles, offering only a modest contribution to the overall base resistance in sands, as has been confirmed by [Han et al. \(2019\)](#) through field tests. Analysis of driving records indicates that a similar system applied to the Wikingier piles, which drove in a fully unplugged coring manner. The IMPACT signal matching code employed by the Authors involved explicit modelling of the internal shaft resistance ([Randolph, 2008](#)). Signal matches in which the ratio of internal-to-external shaft resistance was set between 0 and 0.2 in both the tills and chalk led to the best fits for the cases considered initially. All shaft resistance was considered as applied externally in the final set of analyses reported herein.

The pairs of long-term tension and re-strike tests conducted at WK38, 42 and 70 were planned to allow checking of the static shaft capacities inferred from the dynamic signal matching analyses. Figure 7(a) to (c) presents profiles of the local (equivalent static) shaft resistance,  $\tau_{s,d}$ , interpreted from EOD matches on the six test piles. ‘Static’ EOD shaft resistance appears negligible in the Holocene deposits and varies between 30 and 200kPa in the glacial till, reducing systematically with  $h/R^*$ ; Figure 8. The

WK38 results (Figure 7(a)) indicate significant variations in the glacial till's shaft resistance profiles between identical piles driven at the same location, possibly reflecting locally varying ground conditions, but also demonstrating the degree of variability associated with dynamic test interpretation. Still stronger dependence of  $\tau_{s,d}$  on  $h/R^*$  was observed in the chalk, as illustrated in Figure 7 and Figure 8 with  $\tau_{s,d}$  up to 300kPa on shaft sections close to the tip and minima around 10kPa developing higher on the shaft as the tip advanced. The Chalk's strong  $h/R^*$  dependency reflects its markedly sensitive behaviour. Chalk breaks down readily to putty under laboratory compaction ([Doughty et al., 2018](#)) and this feature has led to piles "running" or falling under their own self weight to considerable depths in chalk without any hammer blows being applied ([Carotenuto et al., 2018](#)). The high density chalk (or Danian Limestone) layer is reflected in the WK70 profile (Figure 7 (c)), where EOD  $\tau_{s,d}$  values reached 80kPa at 10-15m depth, far greater than those in the underlying low-to-medium density chalk.

The EOD shaft capacities assessed from all 12 test piles are summarised in Table 4, along with  $\tau_{avg}$ , the shaft capacities averaged along each pile's length. Here too the  $\tau_{avg}$  values reduce with increasing penetration: the lowest average EOD unit shaft resistance (24kPa) applied to OSS-C2, which had the greatest (36m) penetration into chalk. Figure 7 and Table 4 indicate the significant variations in EOD shaft resistances between nominally identical piles, which range from  $\pm 6\%$  (for WK38) to  $\pm 16\%$  (for WK43).

#### *Dynamic behaviour of aged piles*

The dynamic re-strike tests on aged pre-construction piles, outlined in Table 3, applied three full energy blows with Menck MHU 800S hammer with the Beginning of Restrike (BOR) capacity defined at the first blow. Markedly higher shaft capacities were found than at EOD, as listed in Table 4 and in Table 5, especially at the chalk-dominated WK43 and WK70 locations. The shaft shear stress distributions plotted in Figure 7 add further information on how these gains built up over the pile shafts.

## LONG TERM TESTING

---

### *Static testing procedures*

The seabed static tests were executed by a maintained load procedure with specially developed, remotely-controlled equipment. The system, described by [Barbosa et al. \(2015a\)](#), could apply a maximum tensile load of 15MN and cycle loads with periods of around one minute. Displacements were measured using a Norwegian Geotechnical Institute's (NGI) subsea extensometer system connected to an independent reference frame. Pile failure was defined by either (a) the pile head displacements reaching 137mm ( $D/10$ ) or (b) the semi-logarithmic creep rate,  $k_c$  approaching 4mm/log cycle of time after 30 minutes. Four hydraulic actuators were built into a loading beam linked to two adjacent reaction piles (Figure 9). The load steps included an unload-reload loop, as shown on Figure 10. The load steps were governed by creep rate criteria scaled from the [EA-Pfähle \(2014\)](#) recommendations to reflect pile dimensions and were in keeping with the research methodologies applied by [Chow \(1997\)](#) and [Buckley \(2018\)](#). As discussed later, the frame design was based on capacity predictions that underestimated the chalk's long-term shaft resistances.

### *Glacial till dominated WK38*

The re-strike tests indicated shaft capacities increasing markedly with age. Pile WK38-1, driven to 16.6m through primarily glacial till soils, developed a compressive shaft BOR capacity double that measured on the same pile 108 days earlier at EOD. The parallel tension static load on WK38-2 showed the behaviour depicted in Figure 11, where the static, compressive, shaft capacities interpreted from the dynamic EOD and BOR tests are also marked. The creep displacements observed during maintained load stages followed semi-logarithmic trends with time, developing gradients,  $k_c$  (expressed as mm/log cycle of time) that increased systematically with average mobilised shaft resistance  $\tau_{avg}$  once a 'creep yield' had been exceeded. Figure 12(a) shows that for WK38, creep-yielding took place at around 1/4 of the failure load, when  $\tau_{avg}=30$  kPa, which is referred to as  $\tau_{creep-yield}$ . The logarithmic plot on the right of Figure 12(a) indicates that a power-law relationship applied between  $k_c$  and  $(\tau_{avg}-\tau_{creep-yield})$  for load steps that exceeded the creep yield criterion.

Static tension failure was interpreted at a pile head load of 9.33MN (see Figure 11) and 20.7mm (or 1.5%D) displacement, with  $k_c \approx 3.5\text{mm}/\log$  cycle. Any reverse end-bearing capacity was considered negligible, as all piles were founded into relatively free draining chalk and the testing rates were slow. The net load found after deducting the submerged weight of the soil plug and pile is 8.80MN, giving  $\tau_{avg} = 122\text{kPa}$ .

The static tension capacity proved for WK38 is around 10% lower than the compressive static shaft capacity interpreted from signal matches made for the parallel re-strike test. Relating the tensile static capacity to the compressive (dynamically measured) EOD for the same pile (WK38-2) indicates a combined (glacial till and chalk) shaft set-up factor of 1.65, assuming tension and compressive shaft resistances are equal. Signal matching analysis indicated that 69%, or 6.07MN, of WK38-2's shaft capacity was attributable to the glacial till.

Following full unloading, two ten-cycle packets of one-way axial cyclic loading were applied. The first imposed a Utilisation Ratio (UR = maximum applied cyclic load/static failure load) of 0.62, and the second a UR of 0.84 (Figure 13). The permanent accumulated cyclic displacements,  $s_{acc}$  shown on Figure 14(a), remained below 0.05%D for the first 10 cycles, but increased to 0.07%D/cycle in the second batch giving 1.1%D (or 15mm) of pull-out and cycling halted as cyclic failure appeared imminent. The cyclic loading and unloading stiffnesses ( $k_l$  and  $k_{ul}$ ) are shown on Figure 14(b), normalised by the values developed at N=1. While little stiffness change was observed under the first batch of cycles, the second 10 cycles led to stiffness reductions of 25-35%. Comparably high levels of one-way repetitive tension loading were also able to induce failure with steel piles driven in stiff Cowden glacial sandy clay till; Ove Arup and Partners (1986).

#### *Chalk dominated WK43 and WK70*

The re-strike tests conducted at the chalk-dominated WK43 and WK70 locations showed more marked 'static' shaft capacity set-up. Factors between 5.3 and 5.2 are evident from Table 4, Table 5 and Figure 7. Although variations in base capacity are more difficult to ascertain, signal matching indicated comparatively modest (<20%) changes in base capacity over time. Signal matching for WK43-2 and

WK70-2 indicated that 86% and 96% of the overall shaft capacities developed within the respective piles' chalk sections (see Table 5).

Static load tests on the  $\approx 31\text{m}$  long WK43-2 and WK70-2 piles gave the load-displacement outcomes plotted in Figure 15 and Figure 16 and creep responses illustrated in Figures 12(b) and (c). Both piles manifested clear creep yielding in their maintained load stages. However, neither achieved ultimate failure before the allowable structural limit of the test beam was reached. Methods for extrapolating incomplete pile load tests include the hyperbolic and parabolic load-displacement curve fitting methods of [Brinch Hansen \(1963\)](#), [Chin \(1970\)](#) and [Decourt \(1999\)](#). The power law relationship interpreted between  $k_c$  and  $(\tau_{avg}-\tau_{creep-yield})$  in the WK38 static test (which reached full failure) in Figure 12(a) suggests another approach in which failure can be projected as the point at which the power-law  $k_c$  trend reaches a specified logarithmic creep rate limit. This is taken conservatively here as 3mm/log cycle (an increase on the [EA-Pfähle \(2014\)](#) recommendation of 2mm/log cycle, which reflects the pile dimensions) and then applied in Figure 12(b) and (c). The results from all four extrapolation methods are compared in Table 6. The parabolic and hyperbolic methods led to predictions 14 to 59% higher than the static result for WK38, where full failure was achieved, while the power law  $k_c$ -  $(\tau_{avg}-\tau_{creep-yield})$  extrapolation to 3mm/log cycle matched the static failure load to within 5%. Adopting the latter, locally calibrated, method indicated net tensile static shaft capacities of 20.9MN (or  $\tau_{avg}=158\text{kPa}$ ) at WK43 and 22.44MN ( $\tau_{avg}=168\text{kPa}$ ) at WK70, representing overall set-up factors (for glacial till and chalk) of 4.4 and 4.9 compared to the EOD values. The (compressive) re-strike BOR shaft capacities measured at WK43 and WK70 were 13% lower and 23% higher than the respective extrapolated net tensile failure loads. One of the more conservative alternative extrapolation procedures may have been more applicable to the WK70 case, although this remains unproven. While the dynamic shaft capacities all fall within 23% of the interpreted static values, the estimates for WK43 and WK70 must be treated with caution, as the good agreement proven at the WK38 location is less certain at the chalk dominated profiles.

Adding the WK38 result, the BOR 'static compressive shaft capacities' are on average 5% higher than the tension values assessed from the independent static tests at each location. Given the greater

variability and subjectivity associated with dynamic test interpretation, this degree of correspondence is encouraging: even nominally identical paired piles can show significantly different EOD capacities, as shown in Table 4.

Table 7 presents an overall summary of the interpreted static test results, which are also annotated on Figure 11, Figure 15 and Figure 16. Signal matching for the WK43-2 and WK70-2 BOR tests allowed the respective contributions of the static tension capacities to be estimated as shown in Table 5 where the chalk layers are indicated as providing 18.0MN and 21.5MN of the tension shaft capacities interpreted from the WK43 and WK70 pile tests.

## VARIATIONS IN SHAFT RESISTANCE WITH TIME

---

The shaft resistances interpreted from the BOR blows, as listed in Table 4, can be compared to the final EOD blows to assess changes overtime and Table 5 to 7 confirm marked set-up over the 12 to 15-week post-driving ageing periods. Operational pauses during pile driving provide information on re-strike trends over shorter periods and Table 8 compares the shaft stresses interpreted from the blows applied immediately prior to, and following after, a range of such driving pauses. The combined spread of set-up factors are plotted against time in Figure 17 and Figure 18 for the till and chalk, respectively.

Although pore pressure dissipation was likely to have completed in the tills before the static testing was carried out (15 weeks after driving) shaft capacities may have been continuing to grow through other ageing processes at that stage. The set-up ratios,  $\Lambda$ , of 1.6 to 3.2 achieved up to static testing appeared to follow the approximately semi-logarithmic trend given by Eq. 5 and plotted on Figure 17:

$$\Lambda = \frac{\tau_{avg}(t)}{\tau_{avg}(t = t_{ref})} = 1 + 0.4 \log\left(\frac{t}{t_{ref}}\right) \quad Eq. 5$$

Where  $\tau_{avg}(t)$  is the resistance at time,  $t$  after driving and  $t_{ref}$  is an initial reference time which is taken as 0.01 days. Onshore pile tests in low plasticity clays and sands by [Karlsrud et al. \(2014\)](#) and [Jardine et al. \(2006\)](#) indicated ultimately stable  $\Lambda$  values  $\approx 3$  once six to 12 months had elapsed after driving.



The equivalent chalk set-up trends presented in Figure 18 appear to vary with the degree by which the pile shafts penetrated into the chalk  $L_p^{chalk}$ . Set-up was more marked in cases where more than 20% of the pile was founded in chalk, reflecting greater scope for capacity growth in the high  $h/R^*$  locations where ‘friction fatigue’ losses were most marked during driving. Shaft resistances doubled within ten minutes and re-doubled within 30 minutes, confirming observations made by [Dührkop et al. \(2017\)](#). The set-up tended to stable asymptotes after around 75 days and Eq. 6, a hyperbolic relationship proposed by [Tan et al. \(2004\)](#), appears appropriate, as shown on Figure 18:

$$\Lambda = \frac{\tau_{avg}(t)}{\tau_{avg}(t = t_{ref})} = \Lambda_{ult} \left( m + (1 - m) \left[ \frac{t/T_{50}}{1 + (t/T_{50})} \right] \right) \quad Eq. 6$$

Here  $\Lambda_{ult}$  is the ultimate set up factor,  $T_{50}$  is the time required to reach 50% of  $\Lambda_{ult}$  and  $m$  is a factor applied to improve the early ( $t < 1$  day) age fitting. The  $L_p^{chalk}/L_p > 0.2$  case curve corresponds to  $T_{50}=29$  minutes,  $\Lambda_{ult}=5.6$  and  $m=0.18$ , while that for lower  $L_p^{chalk}/L_p$  ratios employs  $\Lambda_{ult}=2.95$ ,  $T_{50}=100$  minutes and  $m=0.26$ . The dashed line shown on Figure 18 corresponds to an average trend between the two curves. Table 4 indicates that the shaft resistances achieved in the chalk at BOR are significantly higher than those mobilised in the till. Normalising by the relatively low values mobilised during driving leads to higher long-term set-up factors in the chalk layers than in the tills.

Scaling up the pore pressure dissipation times discussed earlier for 43.8mm diameter piezocones by the ratio  $(R^*/R_{cpt})^2$ , where  $D_{cpt}=2R_{cpt}$ , indicates times for 50% pore-water pressure dissipation after installation for 1.37m to 3.7m diameter piles of between 11 and 40 minutes in chalk. Dissipation may therefore be important to the initial part of the set-up trend seen in Figure 18. However, Buckley *et al* ([2018a](#)) hypothesised that an arching mechanism involving drained creep relaxing raised circumferential stresses close to the shaft may also contribute to longer term shaft capacity growth in chalk, as has been postulated previously in sands (e.g. [Chow et al., 1998](#), [White et al., 2005](#), [Jardine et al., 2006](#)). Chemical reactions at the interface, internal re-cementing of the chalk putty and bonding to the interface may also play a role.

Ciavaglia *et al.*’s ([2017](#)) and Buckley *et al.*’s ([2018a](#)) tests on smaller pipe-piles driven in chalk at St. Nicholas-at-Wade indicated similarly shaped set-up curves. However, the smaller onshore piles’

manifested notably slower set-up rates. The Wikingen fractures are closed or tight, water-filled and spaced at 200-600mm (indicating grade A1/A2 chalk), while the St. Nicholas-at-Wade fractures are open to <3mm, air filled and spaced at 60-200mm. The arching mechanism may allow more rapid gains in chalk masses with tight, widely spaced fractures than when fractures are more open and closely spaced. It is also possible that the different groundwater conditions and pile configurations contributed to the onshore piles' slower set-up trends. However, the observation that closed-ended Imperial College Piles installed by slow cyclic jacking at St. Nicholas-at-Wade did not show any shaft capacity increases over extended periods indicates that set-up is strongly dependent on the installation process; see [Buckley \*et al.\* \(2018b\)](#).

## SHORT-TERM STATIC SHAFT CAPACITY PREDICTIONS

---

The end of driving resistances interpreted along the shaft sections installed in chalk exceed significantly the  $\tau_f$  value of 20kPa recommended for static design in CIRIA C574, giving calculated/dynamically-measured  $Q_c/Q_m$  capacity ratios of  $0.64 \pm 0.21$ . The set-up trends discussed above, led to far greater divergence in the long-term tests from CIRIA C574, and lower  $Q_c/Q_m$  ratios. These findings prompted the development of an effective stress-based 'Chalk ICP-18' predictive procedure, which drew on the additional onshore tests on 139mm to 762mm diameter piles, described by [Buckley \*et al.\* \(2018a\)](#) and [Ciavaglia \*et al.\* \(2017\)](#) respectively. Reference was also made to offshore observations for monopile driving in chalk, as described by [Buckley \(2018\)](#) and [Jardine \*et al.\* \(2018\)](#).

The Chalk ICP-18 expressions for driving resistance in low-to-medium density chalk follow the generic ICP-05 ([Jardine \*et al.\*, 2005](#)) approach and, following [Buckley \*et al.\* \(2018a\)](#): (i) rely on CPT tests to account for variations in chalk properties; (ii) capture the marked tendency of radial effective and shear stresses to reduce with  $h/R^*$  and (iii) match the interface-shear failure characteristics observed in instrumented ICP field tests.

Observations involving a wide range of pile diameters and wall thicknesses,  $t_w$  indicated that their  $D/t_w$  ratios affected driving resistance, probably because the puttified chalk annuli's widths depend primarily on  $t_w$ . The outer shaft resistance to driving of open-ended piles (with  $17 < D/t_w < 67$ ) can be matched in

low-medium density chalk by substituting the radial effective stresses given by Eq. 7 into the local Coulomb shaft failure criterion given by Eq. 2 (taking  $\delta' = 33^\circ$  and  $\sigma'_{rf} = \sigma'_{ri}$ ):

$$\sigma'_{ri} = 0.031 q_t \left( \frac{h}{R^*} \right)^{-0.481} \left( \frac{D}{t_w} \right)^{0.145} \quad \text{Eq. 7}$$

For  $h/R^* \geq 6$ .

Eq. 7 aims to capture the radial stress reductions that occur at any given depth as the chalk flows first around the pile tip during continuous driving and then later as the pile tip advances to greater relative depths,  $h$ . [Lehane et al. \(2005\)](#) addressed this for sand by separating out an assumed initial influence of the piles' effective areas from the subsequent 'friction' fatigue by employing independent parameters for each component, while [Lehane et al. \(2013\)](#) retained only the  $h/R^*$  term when dealing with clays. Further disaggregation or other modification of the chalk expressions may be possible as additional data becomes available on installation resistances. Applying the preliminary expression given by Eq. 7 to the nine EOD cases (shown in Table 4) for which CPT data was available in the chalk led to an average  $Q_c/Q_m$  ratio of 0.9 and a standard deviation of 18%. Figure 19 shows examples of the predicted profiles of shaft stress compared with those interpreted from signal matching.

The back-analysis of 70 blows reported in Appendix 3 proceeded by assuming that the piles' base resistances developed over their solid tip areas only during driving and mobilised average annular bearing pressures  $q_{ba}$  that could be related directly to the average local CPT resistance. The latter was characterised as  $q_{t, 1.5D}$ , the mean  $q_t$  averaged 1.5 pile outside diameters ( $D$ ) above and below the tip. The resulting best fit  $q_{ba}/q_{t, 1.5D}$  ratios varied with tip displacement per blow, but indicated a range of  $0.16 < q_{ba}/q_{t, 1.5D} < 0.8$  in both tills and chalk, with a mean around 0.50 and standard deviation  $\approx 0.15$ . No static compression test data is available to assess whether higher ratios might apply in monotonic loading tests that are taken to reach failure after displacements of  $D/10$ , as has been argued for sands by for example [Byrne et al. \(2012\)](#).

## LONG-TERM STATIC SHAFT CAPACITY PREDICTIONS

---

[Buckley \(2018\)](#) and [Jardine \*et al.\* \(2018\)](#) also set out effective stress-based ‘Chalk ICP-18’ predictive expressions for the ‘long-term’ shaft capacities, which are taken as applying 100 or more days after driving. As with the short-term driving case, it is assumed that the Coulomb law applies at the interface (Eq. 2) and that the  $\delta'$  angle can be predicted from appropriate interface shear tests. The static unit shaft shear capacities,  $\tau_f$ , which increase significantly over time, are calculated from expressions that capture the chalks’ constrained interface dilation, which resembles that seen in sands. While it would be attractive to link the short-term and long-term stresses through a simple set-up factor expression, no evidence was found that  $D/t_w$  affected the long-term resistances. It appeared that the long-term shaft resistances could be captured with a simpler independent expression. Under tension or compression loading,  $\sigma'_{rf}$  values applied in Eq. 2 was given as:

$$\sigma'_{rf} = (\sigma'_{rc} + \Delta\sigma'_{rd}) \quad \text{Eq. 8}$$

$$\sigma'_{rc} = 0.081q_t \left( \frac{h}{R^*} \right)^{-0.52} \quad \text{Eq. 9}$$

For  $h/R^* \geq 6$

It was considered that, as in sands (see [Lehane \*et al.\* \(1993\)](#) and [Chow \(1997\)](#) the dilatant  $\Delta\sigma'_{rd}$  component can be estimated, as:

$$\Delta\sigma'_{rd} = \frac{4G\Delta r}{D} \quad \text{Eq. 10}$$

Where  $\Delta r$  is the radial dilation at the interface required to permit failure and the shear modulus,  $G$ , should ideally be measured in the  $G_{hh}$  mode and account for any non-linear dependence on  $\Delta r/D$ . [Buckley \*et al.\* \(2018b\)](#) interpreted a range of radial dilation of 0.23 to 2.04  $\mu\text{m}$  from instrumented ICP tests in chalk and a value of  $\Delta r \approx 0.5 \mu\text{m}$  is recommended in the preliminary Chalk ICP-18 method, which falls far below the peak-to-trough pile shaft roughness measure that is applied in sands, because of the chalk’s far smaller grain sizes. Constrained dilation has a significant effect with small piles, but is predicted to contribute less (<5%) to large diameter offshore piles.

1 While the scalar coefficient (0.081) included in Eq. 9 is notably higher than that expected in sands, the  
2 ‘friction fatigue’ exponent in of 0.52 in Eq. 9 suggests a similar rate of local stress degradation, and  
3 therefore shape of shear stress profile, to that anticipated for silica sands by the ICP-05 and UWA-13  
4 methods.

5 The relative shaft capacity contributions identified from signal matching for the till and chalk layers to  
6 the WK38, 43 and 70 test piles’ shaft capacities allow shaft capacity prediction methods to be assessed  
7 for the chalk and glacial till layers in calculations that are insensitive to the assumptions made in  
8 estimating the minor contributions of the Holocene material, which contributed <0.5% of the long-term  
9 total capacity at WK38, for example. The soil parameter profiles presented earlier (and in the  
10 Appendices) were applied and the ICP-05 sand approach was employed to calculate the minor  
11 contribution of any Holocene cover.

12 Table 9 summarises the outcomes for glacial till shaft capacity contributions interpreted from the  
13 WK38, 43 and 70 tests, as listed in Table 7. Also shown are the predictions made by applying the ICP-  
14 05 sand procedures, which aim to match medium-term (nominally 10 day age) capacities and the API-  
15 2014, Fugro-96, NGI-05, ICP-05 clay and UWA-13 clay methods. The ICP sand method under-predicts  
16 the long-term glacial till resistances by significant margins. However, the piles were tested around 100  
17 days after driving. Open-steel piles tested at comparable ages at Dunkirk ([Jardine et al., 2006](#)) indicated  
18 a set-up factor of  $\approx 1.9$  between their 10 day and 100 day capacities which, if applied to the ICP-05 sand  
19 calculations, raises the predicted-to-measured shaft capacity ratios to  $0.74 < Q_o/Q_m < 1.37$  and gives an  
20 average of 0.96. Adopting any of the cited clay methods leads to large over-predictions for the  
21 resistances available in glacial till units 12-15 weeks after driving, with  $1.5$  (for API-2014)  $< Q_o/Q_m <$   
22  $8.8$  (for UWA13). Surprisingly low average  $\alpha$  values ( $\approx 0.2$  or less) would be needed to obtain matches  
23 with the field capacities. Despite the incomplete drainage seen in the piezocone profiling, the glacial  
24 tills’ appear to have responded to pile driving and testing more like sands than clays, which is consistent  
25 with the classification illustrated on Figure 4 and Figure 6.

26 No fluvioglacial till was present at the static test locations. However, larger diameter production piles  
27 were driven through both the glacial and fluvioglacial till sections considered in Figures 3 to 6. A long-

term re-strike was conducted on one WK42 pile 67 days after driving which provides useful additional evidence. As at the static test locations, signal matching analysis indicated that the sandy glacial till section's contribution exceeded the (nominally ten day age) ICP-05 sand method prediction, giving  $Q_c/Q_m \approx 0.8$ . The ratio could be expected to fall as ageing continues. The clay methods appeared non-conservative again, giving  $Q_c/Q_m$  between 2.1 (for ICP-05 clay) and 8.6 (UWA-13), in keeping with the glacial tills' more sand-like behaviour. Applying clay calculation methods to the lower permeability and higher fines content fluvioglacial section of WK42 indicated  $Q_c/Q_m$  ratios ranging from 0.5 (for NGI-05 and API-14) to 1.2 (UWA-13) with an average of 0.75; the ICP-05 clay method could not be applied as no interface shear tests were available for this unit. However, 10-day age predictions with ICP-05 sand gave  $Q_c/Q_m \approx 0.1$ , confirming that the fluvioglacial till's behaviour was more clay-like than sand-dominated. Caution and field checking are clearly required when designing piles in tills with intermediate sand-to-clay behaviours, such as those encountered at Wikinger.

The equivalent analyses for the piles' chalk layers had to account for the 6.5m thick very high-density chalk, or Danian limestone, layer encountered at WK70. The CIRIA C574 calculation adopted a 'high-density' 120kPa shaft resistance, while  $q_t=50\text{MPa}$  was assumed for the Chalk ICP-18 assessment of WK70's 'limestone' section, matching the operational maximum to which the deployed field CPT equipment operated. Higher  $q_t$  values may have been observed if higher capacity cones had been available.

The outcomes summarised in Table 10 show CIRIA C574 to be markedly over-conservative at all three test sites, with  $Q_c/Q_m$  outcomes between 5 and 10. In contrast, the Chalk ICP-18 expressions matched the test capacities to within +/-20%. Further independent checking is required as the latter approach was developed to fit the field behaviour observed at Wikinger and St Nicholas-at-Wade. It is encouraging that Buckley (2018) and [Jardine et al. \(2018\)](#) found fair capacity matches for other sites where the necessary CPT profiles and test records are available, including closed-ended piles installed by impact driving. [Jardine et al. \(2019\)](#) describe research that is underway to develop the method further. However, Chalk ICP-18 must be regarded as a preliminary proposal that may well require updating as new findings emerge.

## SUMMARY & CONCLUSIONS

---

High costs and logistical difficulties have led to offshore static pile load testing and/or long-term dynamic re-strike testing being extremely rare. However, the Wiking case history shows that field testing can be highly cost-effective, provided it is conducted in advance of final design. [Barbosa \*et al.\* \(2017\)](#) describe how major project risks were eliminated and total pile lengths reduced by 3km for Wiking, saving 8,000 tonnes of steel and 16,000 tonnes of CO<sub>2</sub> emissions. Large sums were recouped from supply, fabrication and installation costs. Highly significant benefits may be taken from considering ageing trends in both tills and chalk, provided the piles can be driven well before they have to carry their design loads. Still greater structural savings could have been achieved at Wiking if the testing had been conducted at an even earlier stage.

Parallel industrial-academic research, including pile experiments at an onshore site, laboratory testing and analysis aided the interpretation of the novel Wiking field tests and helped to frame ten main conclusions regarding piles driven in dense/stiff low plasticity tills and low-medium density chalk:

1. Static testing leads to more reliable measurements of pile capacity than the more complex and less objective process of analysing instrumented hammer blows dynamically. However, careful signal matching of pile monitoring data and analysis of static tension tests conducted at Wiking led to broadly compatible field measurements;
2. The piles' shaft resistances apply principally on their outside areas during driving and re-striking. The local shaft shear stresses reduce markedly with increasing relative tip penetration ( $h/R^*$ ) in tills and, still more sharply, in chalk;
3. Shaft capacity set-up progressed gradually in the tills, leading after 15 weeks to resistances around 2.4 (+/-0.8) times those available at the end-of-driving;
4. More significant shaft increases applied in chalk, with average ultimate set-up factors greater than 5.5 that followed a hyperbolic trend with time and depended on  $h/R^*$ . Smaller factors applied to piles with relatively low penetrations into the chalk;

- 1        5. Independent dynamic and full static tests to failure conducted on one pair of offshore piles  
2        showed good agreement regarding overall shaft capacity. Signal matching analyses also  
3        allowed robust estimates to be made of how the piles' long-term (108-day age) shaft  
4        capacities were distributed between the till and chalk layers. Although subject to greater  
5        uncertainty, the capacities interpreted from dynamic restrikes added value at two other  
6        chalk-dominated sites where the static tests did not reach full failure;
- 7        6. The integrated programme of static and dynamic testing indicated that the shaft capacities  
8        developed in the tills were highly sensitive to local clay content and permeability. The low  
9        plasticity glacial till's interpreted long-term shaft capacity contributions were broadly  
10       compatible with estimates made with the ICP-05 sand approach, when allowance was made  
11       for the test piles' ages. However, they fell far below predictions made with five offshore  
12       design methods for clays. In contrast, re-strike test analysis involving the higher clay  
13       content and lower permeability fluvioglacial layers indicated both better correspondence  
14       with clay method predictions and resistances far higher than expected by the ICP-05 sand  
15       method;
- 16       7. The CIRIA C574 shaft capacity method significantly underpredicted the driving resistance  
17       experienced in the chalk and greatly underestimated, by factors of 5 to 10, the 100-day age  
18       shaft capacities.
- 19       8. The Chalk ICP-18 expressions for driving resistance led to good representations of overall  
20       field capacities at end of installation and captured the chalk's marked  $h/R^*$  trends. The  
21       long-term shaft capacity expressions reflected equally well the field capacities observed at  
22       ages exceeding 100 days.
- 23       9. The results have important economic consequences for projects such as large offshore  
24       windfarms. Full scale static testing was shown to be feasible offshore and highly cost-  
25       effective to the Wiking project. Highly significant benefits may be taken by recognising  
26       the favourable effects of pile ageing, updating design procedures and supporting  
27       engineering assessments through careful field checking.



1           10. Independent checking of the preliminary Chalk ICP-18 approach at other sites has given  
2           encouraging results. New research is underway to help further refine the approach.

3  
4   **ACKNOWLEDGEMENTS**

---

5   The Authors acknowledge gratefully the major funding from Innovate-UK (Grant No. 101968) to  
6   undertake the research described, as well as Bilfinger Construction GmbH (Principal Contractor) and  
7   Allnamics Geotechnical B.V. who carried out the pile testing. The Authors are also grateful Professor  
8   Barry Lehane for his useful correspondence and Professor Mark Randolph for the use of IMPACT.  
9   They also acknowledge the work of Gardline Geosciences Ltd., GEO Copenhagen and Fugro  
10   Geoconsulting Ltd in their site investigations and laboratory testing.

## REFERENCES

---

- Addis M. & Jones, M. (1990). Mechanical behaviour and strain rate dependance of high porosity chalk. *Proc. Intl. Chalk Symposium*, Brighton, UK: 239-244
- Al-Shafei K., Cox, W. & Helfrich, S. (1994). Pile load tests in dense sand: Analysis of static test results. *Offshore Technology Conference*, Houston, Texas: 83-103
- Alves A. M., Lopes, F. R., Randolph, M. F. & Danziger, B. R. (2009). Investigations on the dynamic behavior of a small-diameter pile driven in soft clay. *Can. Geotech. J.*, **46**, No. 12: 1418-1430
- API (2014). API RP 2A-WSD:Recommended practice for planning, designing and constructing fixed offshore platforms – working stress design, 22nd edition, American Petroleum Institute
- Augustesen A. H., Leth, C. T., Ostergaard, M. U., Moller, M., Dührkop, J. & Barbosa, P. (2015). Design methodology for cyclically and axially loaded piles in chalk for Wikingen OWF. *Proc. Frontiers in Offshore Geotechnics III*, Oslo, Norway: 509-514
- Baldi G., Bellotti, R., Ghionna, V. N., Jamiolkowski, M. & Lo Presti, D. C. F. (1989). Modulus of sands from CPTs and DMTs. *Proc. 12th Intl. Conf. Soil Mech. Found. Eng.*: 165-170
- Barbosa P., Geduhn, M., Jardine, R. J., Schroeder, F. C. & Horn, M. (2015a). Offshore pile load tests in chalk. *Proc. 16th Eur. Conf. Soil Mech. Geotech. Eng.*, Edinburgh, Scotland: 2885-2890
- Barbosa P., Geduhn, M., Jardine, R. J. & Schroeder, F. C. (2015b). Full scale offshore verification of axial pile design in chalk. *Proc. Frontiers in Offshore Geotechnics III*, Oslo, Norway: 516-520
- Barbosa P. M., Geduhn, M., Jardine, R. J. & Schroeder, F. C. (2017). Large scale offshore static pile tests-practicality and benefits. *Proc. 8th Int. Conf. on Offshore Site Investigation and Geotechnics*, London, UK: 644-651
- Bishop A. W., Green, G., Garga, V. K., Andresen, A. & Brown, J. (1971). A new ring shear apparatus and its application to the measurement of residual strength. *Géotechnique*, **21**, No. 4: 273-328
- Bowden A. J., Spink, T. W. & Mortimore, R. N. (2002). The engineering description of chalk: its strength, hardness and density. *Q. J. Eng. Geol. Hydrogeol.*, **35**, No. 4: 355-361
- Brinch Hansen J. (1963). Discussion: Hyperbolic Stress Strain Response: Cohesive Soils. *J. Soil Mech. Found. Div. - ASCE*, **89**, No. 4: 241-242
- Brown M. J. & Hyde, A. F. L. (2008). Rate effects from pile shaft resistance measurements. *Canadian Geotechnical Journal*, **45**, No. 3: 425-431
- BSH (2015). Minimum requirements concerning the constructive design of offshore structures within the Exclusive Economic Zone (EEZ), Bundesamt für Seeschifffahrt
- Buckley R. M., Kontoe, S., Jardine, R. J., Maron, M., Schroeder, F. C. & Barbosa, P. (2017). Common pitfalls of pile driving resistance analysis - A case study of the Wikingen offshore windfarm. *Proc. 8th Intl. Conf. Offshore Site Investigation and Geotechnics*, London, UK: 1246-1253
- Buckley R. M., Jardine, R. J., Kontoe, S., Parker, D. & Schroeder, F. C. (2018a). Ageing and cyclic behaviour of axially loaded piles driven in chalk. *Géotechnique*, **68**, No. 2, <https://doi.org/10.1680/jgeot.17.P.012>: 146-161
- Buckley R. M., Jardine, R. J., Kontoe, S. & Lehane, B. M. (2018b). Effective stress regime around a jacked steel pile during installation ageing and load testing in chalk. *Can. Geotech. J.* doi: 10.1139/cgj-2017-0145, **55**, No. 11: 1577-1591
- Buckley R. M. (2018). *The axial behaviour of displacement piles in chalk*. PhD Thesis, Imperial College London, London, UK

- Byrne T., Doherty, P., Gavin, K. & Overy, R. (2012). Comparison of Pile Driveability Methods In North Sea Sand. *Proc. 7th Intl Conf. Offshore Site Investigations and Geotechnics*, London, UK: 481-488
- Cambridge-Insitu (2013). *Wiking Offshore Wind Farm Ground Investigation 2013 - Results of Pressuremeter tests* Cambridge Insitu Ltd, CIR1286/13
- Carotenuto P., Meyer, V., Strøm, P. J., Cabarkapa, Z., St. John, H. & Jardine, R. J. (2018). Installation and axial capacity of the Sheringham Shoal offshore wind farm monopiles – a case history. *Engineering in Chalk*, London, UK: 117-122
- Chan L. D., Buckley, R. M., Liu, T. & Jardine, R. J. (2019). Laboratory investigation of interface shearing in chalk. *Proc. 7th International Symposium on Deformation Characteristics of Geomaterials - in press*, Glasgow, UK:
- Chin F. K. (1970). Estimation of the ultimate load of piles not carried to failure. *Proc. 2nd Southeast Asian Conf. on Soil Eng.*, Singapore: 81-92
- Chin F. K. (1971). Discussion: Pile Tests—Arkansas River Project. *J. Soil Mech. Found. Div. - ASCE*, **97**, No. 6: 930-932
- Chow F. C. (1997). *Investigations into Displacement Pile Behaviour for Offshore Foundations*. PhD Thesis, Imperial College London, London, UK
- Chow F. C., Jardine, R. J., Brucy, F. & Nauroy, J. F. (1998). Effects of time on capacity of pipe piles in dense marine sand. *J. Geotech. Geoenviron. Eng. - ASCE*, **124**, No. 3: 254-264
- Ciavaglia F., Carey, J. & Diambra, A. (2017). Time-dependent uplift capacity of driven piles in low to medium density chalk. *Géotechnique Letters*, **7**, No. March: 1-7
- CIJV (2013). *Wiking offshore windfarm: Geotechnical Site Survey Report based on main geotechnical campaign*, COWI/IMS Joint Venture, A031412-005-RP
- CIJV (2014a). *Wiking offshore windfarm: soil and foundation expertise report based on main geotechnical campaign*, COWI/IMS Joint Venture, WIK-CIJV-IB-0488
- CIJV (2014b). *Pile Load Test Concept Based on Geotechnical Main Campaign*, COWI/IMS Joint Venture, WIK-CIV-IB-0816
- Clarke J., Long, M. & Hamilton, J. (1993). The axial tension test of an instrumented pile in overconsolidated clay at Tilbrook Grange. *Large-scale pile tests in clay*. Thomas Telford Publishing: 362-380
- Clayton C. R. I. (1978). *Chalk as Fill*. PhD Thesis, University of Surrey, Surrey, UK
- Decourt L. (1999). Behavior of foundations under working load conditions. *Proc. 11th Pan-American Conf. Soil Mech. and Geot. Eng.*, Foz do Iguassu, Brazil: 453-488
- Deeks A. J. & Randolph, M. F. (1995). A simple model for inelastic footing response to transient loading. *Int. J. Num. Meth. Geotech. Eng.*, **19**, No. 5: 307-329
- DIN (2009). DIN-EN-1997-1: Eurocode 7: Geotechnical Design - Part 1: General rules; English version, DIN
- DIN (2012). DIN-1054 Subsoil: Verification of the safety of earthworks and foundations, Supplementary rules to DIN EN 1997-1, DIN
- Doughty L. (2016). *Laboratory testing of chalk*. MSc Thesis, Imperial College London, London, UK
- Doughty L. J., Buckley, R. M. & Jardine, R. J. (2018). Investigating the effect of ageing on the behaviour of chalk putty. *Engineering in Chalk*, London, UK: 695-701
- Dührkop J., Maretzki, S. & Rieser, J. (2017). Re-evaluation of pile driveability in chalk. *Proc. 8th Intl. Conf. Offshore Site Investigation and Geotechnics* London, UK: 666-673

- EA-Pfähle (2014). *Recommendations on Piling: Piling Committee of the German Geotechnical Society (abbreviated as: EA Pfähle)*, Germany: John Wiley & Sons.
- Fugro (2013). *Wiking Offshore Windfarm: Advanced Laboratory and Drivability Assessment*, Fugro Geoconsulting Ltd., J22026-1
- Gavin K. & Lehane, B. M. (2007). Base load-displacement response of piles in sand. *Can. Geotech. J.*, **44**, No. 9: 1053-1063
- Gens A. (1982). *Stress-strain and strength characteristics of a low plasticity clay*. PhD Thesis, Imperial College London (University of London), London, UK
- Hamre L. (2018). *Typical monopile sizes*.
- Han F., Ganju, E., Prezzi, M., Salgado, R. & Zaheer, M. (2019). Axial resistance of open-ended pipe pile driven in gravelly sand. *Géotechnique*, (in press). .
- ISO (2007). 19902: 2008-07: Petroleum and natural gas industries—Fixed steel offshore structures. 1st Edition, International Standards Organisation
- Iverson N. R., Hooyer, T. S. & Baker, R. W. (1998). Ring-shear studies of till deformation: Coulomb-plastic behavior and distributed strain in glacier beds. *Journal of Glaciology*, **44**, No. 148: 634-642
- Jardine R. J., Brooks, N. J. & Smith, P. R. (1985). The use of electrolevel transducers for strain measurements in triaxial tests on weak rock. *Int. J. Rock Mech. Min. Sci. & Geomech. Abstr.*, **22**, No. 5: 331-337
- Jardine R. J. (1985). *Investigations of pile-soil behaviour, with special reference to the foundations of offshore structures*. PhD Thesis, Imperial College London (University of London), London, UK
- Jardine R. J., Chow, F. C., Overy, R. & Standing, J. R. (2005). *ICP design methods for driven piles in sands and clays*, London: Thomas Telford.
- Jardine R. J., Standing, J. R. & Chow, F. C. (2006). Some observations of the effects of time on the capacity of piles driven in sand. *Géotechnique*, **56**, No. 4: 227-244
- Jardine R. J., Buckley, R. M., Kontoe, S., Barbosa, P. & Schroeder, F. C. (2018). Behaviour of piles driven in chalk. *Engineering in Chalk*. ICE Publishing: 33-51
- Jardine R. J., Buckley, R. M., Byrne, B., Kontoe, S., Macadam, R. & Vinck, K. (2019). The ALPACA research project to improve driven pile design in Chalk. *Proc. 17th European Conference on Soil Mechanics and Geotechnical Engineering, in preparation*, Reykjavik, Iceland:
- Jardine R. J. (2019). Geotechnics and Energy: 56th Rankine Lecture. *Géotechnique, to appear*.
- Karlsrud K., Clausen, C. & Aas, P. (2005). Bearing capacity of driven piles in clay, the NGI approach. *Proc. Intl. Symp. Frontiers in Offshore Geotechnics*, Perth, Australia: 775-782
- Karlsrud K., Jensen, T. G., Lied, E. K. W., Nowacki, F. & Simonsen, A. S. (2014). Significant ageing effects for axially loaded piles in sand and clay verified by new field load tests. *Offshore Technology Conference*, Houston, Texas: 1-19
- Kolk H. & der Velde, E. (1996). A reliable method to determine friction capacity of piles driven into clays. *Offshore Technology Conference*, Houston, Texas: 337-346
- Lahrs T. & Kallias, A. (2013). Probelastungen von Stahlrohren in Kreide für den Offshore-Windpark Baltic 2. *Proc. Pfahl Symposium*, Braunschweig, Germany: 451-466
- Le T. M. H., Eiksund, G. R. & Strøm, P. J. (2014). Characterisation of Residual Shear Strength at the Sheringham Shoal Offshore Wind Farm. *Proc. 33rd Intl. Conf. Ocean, Offshore and Arctic Eng.*, San Francisco, California: 1-9

- Leddra M. J., Jones, M. E. & Goldsmith, A. S. (1993). Compaction and shear deformation of a weakly-cemented, high porosity sedimentary rock. *The Engineering Geology of Weak Rock*, Leeds, UK 45-54
- Lee S. L., Chow, Y. K., Karunaratne, G. P. & Wong, K. Y. (1988). Rational wave equation model for pile-driving analysis. *J. Geotech. Eng. - ASCE*, **114**, No. 3: 306-325
- Lehane B. M. (1992). *Experimental Investigations of Pile Behaviour using Instrumented Field Piles*. PhD Thesis, Imperial College London, London, UK
- Lehane B. M., Jardine, R. J., Bond, A. J. & Frank, R. (1993). Mechanisms of shaft friction in sand from instrumented pile tests. *J. Geotech. Eng - ASCE*, **119**, No. 1: 19-35
- Lehane B. M. & Jardine, R. J. (1994). Displacement pile behaviour in glacial clay. *Can. Geotech. J.*, **31**, No. 1: 79-90
- Lehane B. M., Schneider, J. A. & Xu, X. (2005). The UWA-05 method for prediction of axial capacity of driven piles in sand. *Proc. 1st Intl. Symp. Frontiers in Offshore Geotechnics*, Perth, Australia: 683-689
- Lehane B. M., Li, Y. & Williams, R. (2013). Shaft capacity of displacement piles in clay using the cone penetration test. *J. Geotech. Geoenviron. Eng. - ASCE*, **139**, No. 2: 253-266
- Lehane B. M., Lim, J. K., Carotenuto, P., Nadim, F., Lacasse, S., Jardine, R. J. & van Dijk, B. (2017). Characteristics of unified databases for driven piles. *Proc. 8th Intl. Conf. Offshore Site Investigation and Geotechnics*, London, UK: 162-194
- Long M. & Menkiti, C. O. (2007). Geotechnical properties of Dublin boulder clay. *Géotechnique*, **57**, No. 7: 595-611
- Lord J. A., Clayton, C. R. I. & Mortimore, R. N. (2002). *Engineering in chalk*, CIRIA, C574
- Loukidis D., Salgado, R. & Abou-Jaoude, G. (2008). *Assessment of Axially-Loaded Pile Dynamic Design Methods and Review of INDOT Axially-Loaded Design Procedure*, Purdue University, FHWA, FHWA/IN/JTRP-2008/6
- Matthews M. C. & Clayton, C. R. I. (1993). Influence of intact porosity on the engineering properties of a weak rock. *Intl. Symp. Geotechnical Engineering of Hard Soils and Soft Rocks*, Rotterdam, the Netherlands: 693-702
- Mayne P. W. & Rix, G. J. (1993). G max-qc relationships for clays. *Geotech. Test. J.*, **16**, No. 1: 54-60
- McAdam R. A., Byrne, B. W., Houlsby, G. T., Beuckelaers, W. J. A. P., Burd, H. J., Gavin, K., Igoe, D., Jardine, R. J., Martin, C. M., Muir Wood, A., Potts, D. M., Skov Gretlund, J., Taborda, D. M. G. & Zdravković, L. (2018). Monotonic lateral loaded pile testing in a dense marine sand at Dunkirk, *Géotechnique*, *in press*.
- McGann C. R., Bradley, B. A., Taylor, M. L., Wotherspoon, L. M. & Cubrinovski, M. (2015). Applicability of existing empirical shear wave velocity correlations to seismic cone penetration test data in Christchurch New Zealand. *Soil Dynamics and Earthquake Engineering*, **75**, No.: 76-86
- Obst K., Nachtweide, C. & Müller, U. (2017). Late Saalian and Weichselian glaciations in the German Baltic Sea documented by Pleistocene successions at the southeastern margin of the Arkona Basin. *Boreas*, **46**, No. 1: 18-33
- Ove-Arup&Partners (1986). *Research on the behavior of piles as anchors for buoyant structures—Summary report*. Dept of Energy, Offshore Technology Report, OTH 86 215
- PISA (2015). *Pisa Project - Field Test Factual Report* Revision B
- Randolph M. F. & Wroth, C. P. (1979). An analytical solution for the consolidation around a driven pile. *Intl. J. Numer. Anal. Methods Geomech.*, **3**, No. 3: 217-229

- Randolph M. F. & Simons, H. A. (1986). An improved soil model for one-dimensional pile driving analysis. *Proc. 3rd Intl. Conf. Numerical Methods in Offshore Piling*, Nantes, France: 3-17
- Randolph M. F. (1993). Analysis of stress-wave data from pile tests at Pentre and Tilbrook. *Large-scale pile tests in clay*, 1993 London. pp.^
- Randolph M. F. (2003). Science and empiricism in pile foundation design. *Géotechnique*, **53**, No. 10: 847-875
- Randolph M. F. (2008). *IMPACT - Dynamic analysis of pile driving*, Manual
- Razoaki R. N. (2000). *Effect of ageing on mechanics of chalk slurries*. PhD Thesis, University of Portsmouth, Portsmouth, UK
- Robertson P. K. (1990). Soil classification using the cone penetration test. *Canadian Geotechnical Journal*, **27**, No. 1: 151-158
- Salgado R., Loukidis, D., Abou-Jaoude, G. & Zhang, Y. (2015). The role of soil stiffness non-linearity in 1D pile driving simulations. *Géotechnique*, **65**, No. 3: 169-187
- Skov R. & Denver, H. (1988). Time-dependence of bearing capacity of piles. *Proc. 3rd Int. Conf. on the Application of Stress-Wave Theory to Piles*, Ottawa, Canada: 879-888
- Smith A. K. C. (2001). Interpretation of cone penetration tests in chalk. *Ground Engineering*, **34**, No. 9: 30-35
- Tan S. L., Cuthbertson, J. & Kimmerling, R. E. (2004). Prediction of pile set-up in non-cohesive soils. *Current practices and future trends in deep foundations: Contributions in Honor of George G. Gobel*, Los Angeles, California, USA: 50-65
- Ushev E. (2018). *Laboratory investigation of the mechanical properties of cowden till under static and cyclic conditions*. PhD Thesis, London, UK
- Weltman A. & Healy, P. (1978). *Piling in 'Boulder Clay' and other Glacial Tills DoE / CIRIA Report PG 5*,
- White D. J., Schneider, J. A. & Lehane, B. M. (2005). The influence of effective area ratio on shaft friction of displacement piles in sand. *Proceedings of the 1st International Symposium on Frontiers in Offshore Geotechnics, ISFOG 2005*, 2005. pp 741-748.^
- Xu X., Liu, H. & Lehane, B. M. (2006). Pipe pile installation effects in soft clay. *Proc. of the ICE Geotech. Eng.*, **159**, No. 4: 285-296
- Ziogos A., Brown, M., Ivanovic, A. & Morgan, N. (2017). Chalk-steel interface testing for marine energy foundations. *Proc. of the ICE Geotech. Eng.*, **170**, No. 3: 285-298

## NOTATION

---

### Roman Alphabet

$a$	Cone area ratio
$C_b$	Base dashpot constant (dynamic soil resistance models)
$C_c$	Compression index
$C_s$	Shaft dashpot constant (dynamic soil resistance models)
$c'$	Effective cohesion intercept
$c_h$	Coefficient of horizontal consolidation
$D$	Diameter of pile
$F$	Force in the pile
$F_{up}$	Upward travelling wave
$f_s$	CPT sleeve friction
$G$	Shear modulus
$G_{max}$	Maximum shear modulus
$G_s$	Specific gravity
$G_{hh}$	Shear modulus (propagating horizontally and polarised horizontally)
$G_{vh}$	Shear modulus (propagating vertically and polarised horizontally)
$G_1$	Secant shear modulus
$h$	Distance from the pile tip
$I_r$	Rigidity index = $G/s_u$
$K_b$	Base spring constant (dynamic soil resistance models)
$K_c$	Coefficient of radial effective stress (shaft) after full equalisation = $\sigma'_{rc}/\sigma'_{vo}$
$K_s$	Shaft spring constant (dynamic soil resistance models)
$K_0$	Coefficient of earth pressure at rest ( <i>in-situ</i> )
$k_l$	Cyclic loading stiffness
$k_{ul}$	Cyclic unloading stiffness
$k_c$	Displacement creep rate
$L_p$	Length of pile penetration
$L_p^{chalk}$	Length of pile penetration in chalk
$M$	Empirical parameter used to assess set up factor in <a href="#">Skov and Denver (1988)</a> equation
$M_{tc}$	Stress ratio at critical state in triaxial stress space
$m$	Empirical parameter used to assess set up factor in <a href="#">Tan et al. (2004)</a> equation
$m_0$	Supplementary lumped mass connected through pile base node
$N$	Number of axial cycles applied
$p'$	Mean effective stress
$p_a$	Atmospheric pressure
$Q_b$	Pile base axial load resistance (capacity)
$Q_s$	Pile shaft axial load resistance (capacity)
$Q_{tot}$	Pile total axial load resistance (capacity)

$q_{ba}$	Pile end-bearing resistance under annulus
$q_{b,stat}$	Limit base stress plastic slider (dynamic soil resistance model)
$q_{b,0.1D}$	Pile end-bearing unit resistance at a displacement of 10% the pile diameter
$q_t$	Total cone resistance ( $=q_c+(1-a)u_2$ )
$q_{t,1.5D}$	Average net CPT tip resistance $\pm 1.5D$ around pile base
$q_u$	Unconfined compressive strength
$R$	Pile radius
$R_a$	Average centre line roughness
$R_i$	Internal pile radius
$R_{t,c}$	Designer's characteristic tensile capacity
$R^*$	Equivalent radius for open-ended piles
$S_t$	Sensitivity
$s_{acc}$	Accumulated permanent cyclic displacement
$s_u$	Undrained shear strength
$T$	Dimensionless time factor
$T_{50}$	Time to achieve 50% of ultimate pile set-up
$t$	Time
$t_{ref}$	Reference time to assess pile ageing
$t_w$	Pile wall thickness
$t_{50}$	Time for 50% dissipation of excess pore water pressures in a CPT dissipation test
$u_2$	CPT excess pore water pressures measured at the shoulder position
$V_s$	Elastic shear wave velocity
$V_p$	Elastic compression wave velocity
$v$	Velocity
$v_0$	Reference velocity ( $=1\text{m/s}$ )
$w$	Displacement
$w_c$	Water content
$w_l$	Liquid limit
$w_{pl}$	Plastic limit
$w_{sat}$	Saturation moisture content
$Z$	Pile impedance
$z$	Depth

### Greek alphabet

$\alpha$	$\alpha$ -type driven pile design method factor
$\alpha_s$	Shaft viscosity parameter (soil resistance model)
$\beta_s$	Shaft viscosity parameter (soil resistance model)
$\Gamma$	Specific volume on the critical state line at $p' = 1\text{kPa}$
$\gamma_{bulk}$	Bulk density
$\gamma_d$	Dry density



$\Delta h$	Change in sample height during shearing
$\Delta r$	Average movement of the soil grains due to dilation
$\Delta v$	Relative velocity between the pile and soil
$\Delta \sigma'_{rd}$	change of radial effective stress during shearing due to dilation
$\delta'$	Interface angle of shearing resistance
$\delta'_f$	Failure interface angle of shearing resistance
$\delta'_{peak}$	Peak interface angle of shearing resistance
$\delta'_{ult}$	Ultimate interface angle of shearing resistance
$\Lambda$	Set-up factor on shaft capacity
$\Lambda_{ult}$	Ultimate set-up factor on shaft capacity
$\lambda$	Slope of the isotropic compression line
$N$	Specific volume on the NCL at $p'=1\text{kPa}$
$\rho_s$	Soil or chalk mass density
$\sigma'_{ri}$	Short-term radial effective stresses
$\sigma'_{rc}$	Radial effective stress after equalisation
$\sigma'_{rf}$	Radial effective stress at failure
$\sigma'_{v0}$	Vertical effective stress
$\sigma'_{vy}$	Vertical yield stress
$\tau_{avg}$	Average shaft shear stress at failure from static or dynamic test
$\tau_{avg}(t)$	Average shaft shear stress at failure from static or dynamic test at time $t$
$\tau_{creep-yield}$	Average shaft shear stress below which static test creep rates are negligible
$\tau_{inter}$	Limit shaft shear stress at low strain rates (dynamic soil resistance model)
$\tau_f$	Calculated long-term local shear stress at static failure from design methods
$\tau_{s,d}$	Local shear stress at failure interpreted from dynamic tests
$\tau_{stat}$	Limit shear stress plastic slider (dynamic soil resistance model)
$\nu$	Poisson's ratio
$\varphi'$	Angle of shearing resistance
$\varphi'_{cv}$	Angle of shearing resistance at critical state

## Abbreviations

API	American petroleum institute
BOR	Beginning of restrike
BSH	Bundesamt für Seeschifffahrt und Hydrographie
CAU	Consolidated anistropically undrained triaxial test
CIRIA	Construction industry research and information association
CPT	Cone penetration resistance
CYC	Cyclic load test
DPT	Dynamic pile test

EC7	Eurocode 7
EOD	End of driving
IDD	Intact dry density
ISO	International standards organisation
NC	Normally consolidated
OCR	Overconsolidation ratio
OSS	Offshore substation
SLT	Static load test
UCS	Unconfined compressive strength
UR	Utilisation ratio
UU	Unconsolidated undrained triaxial test
WTG	Wind turbine generator
YSR	Yield stress ratio or apparent overconsolidation ratio
Z <sub>v</sub>	Velocity times impedance

## LIST OF FIGURES

---

Figure 1 Plan showing relative layout of test piles, boreholes and cone penetration tests at each pre-construction test location (a) WK38 (b) WK43 (c) WK70 Note: each plan based on arbitrary site datum position

Figure 2 Shear modulus,  $G_{vh}$  in chalk from suspension P-S logging at the test sites (mbsb=metres below sea bed)

Figure 3 Site profiles at test sites (a) WK38 (b) WK42 (c) WK43 (d) WK70

Figure 4 Profiles of soil behaviour type index,  $I_c$  (Robertson, 1990), undrained shear strength,  $s_u$  calculated from the CPT cone resistance assuming clay behaviour and an  $N_{kt}$  factor of 22.5 and Yield Stress Ratio at (a) WK38 and WK42 (b) WK43 and WK70

Figure 5 Correlation between cone resistances and shear wave velocity in chalk developed from the results at eight WK test locations (a) cone resistance,  $q_t$  versus shear wave velocity  $V_s$  (b) measured versus calculated  $q_t$

Figure 6 Particle size distributions in fluvioglacial and glacial till

Figure 7 Compressive shaft resistance back analysed using IMPACT at end of driving and beginning of restrike (a) WK38 (b) WK43 (c) WK70

Figure 8 Illustration of dependence of compressive shaft resistance on  $h/R^*$  (a) mid driving blows during installation of WK38-1 (b) mid driving blows during installation of WK38-2 (c) mid driving blows during installation of WK70-2 (d) mid driving blows during installation of OSS-C4

Figure 9 Schematic of loading frame and reaction pile arrangement for subsea static load tests at Wikingen; after Barbosa et al. (2015a)

Figure 10 Static test loading procedure for offshore tests at Wikingen for loading up to 15MN (where  $R_{ic}$  is the characteristic design load)

Figure 11 Load – displacement behaviour during static axial tension test WK38-2\_SLT\_108

Figure 12 Extrapolation of creep rates to failure (a) WK38-2 (b) WK43-2 (c) WK70-2.  $\tau_{avg} - \tau_{creep-yield}$  is limit below which the creep rates were negligible

Figure 13 Average shaft resistance mobilised during WK38-2\_CYC\_108 versus time

Figure 14 WK38-2\_CYC\_108 (a) permanent cyclic displacements normalised by pile diameter (b) cyclic loading and unloading stiffness

Figure 15 Load – displacement behaviour and extrapolated failure load during static axial tension test on WK43-2

Figure 16 Load – displacement behaviour and extrapolated failure load during static axial tension test on WK70-2

Figure 17 Set-up trends in glacial till from dynamic restrike tests and from blows following driving pauses with semi- logarithmic capacity increase trend without apparent asymptotic value over monitoring period

Figure 18 Set-up factors in chalk from dynamic restrike tests and from blows following driving pauses with interpreted trends for high and low  $h/R^*$  values

Figure 19 Examples of shear stress profiles at EOD interpreted from signal matching; profiles predicted using Eq. 7 and Eq. 2

Figure 20: Triaxial tests on samples of intact structured and structureless chalk (a) effective stress paths (b) deviator stress versus axial strain (tests conducted by GEO)

Figure 21: CAU triaxial tests on samples of glacial till (a) effective stress paths (b)  $q/p'$  versus axial strain (tests conducted by GEO)

Figure 22: Ring shear tests on samples of glacial till conducted at Imperial College (a) interface friction angle versus displacement (b) change in sample thickness versus displacement (Buckley, 2018)

Figure 23: Example signal match from blow WK38-2\_DPT\_EOD: measured and calculated (a) force and velocity times impedance (b) upward travelling force (c) displacement

## FIGURES

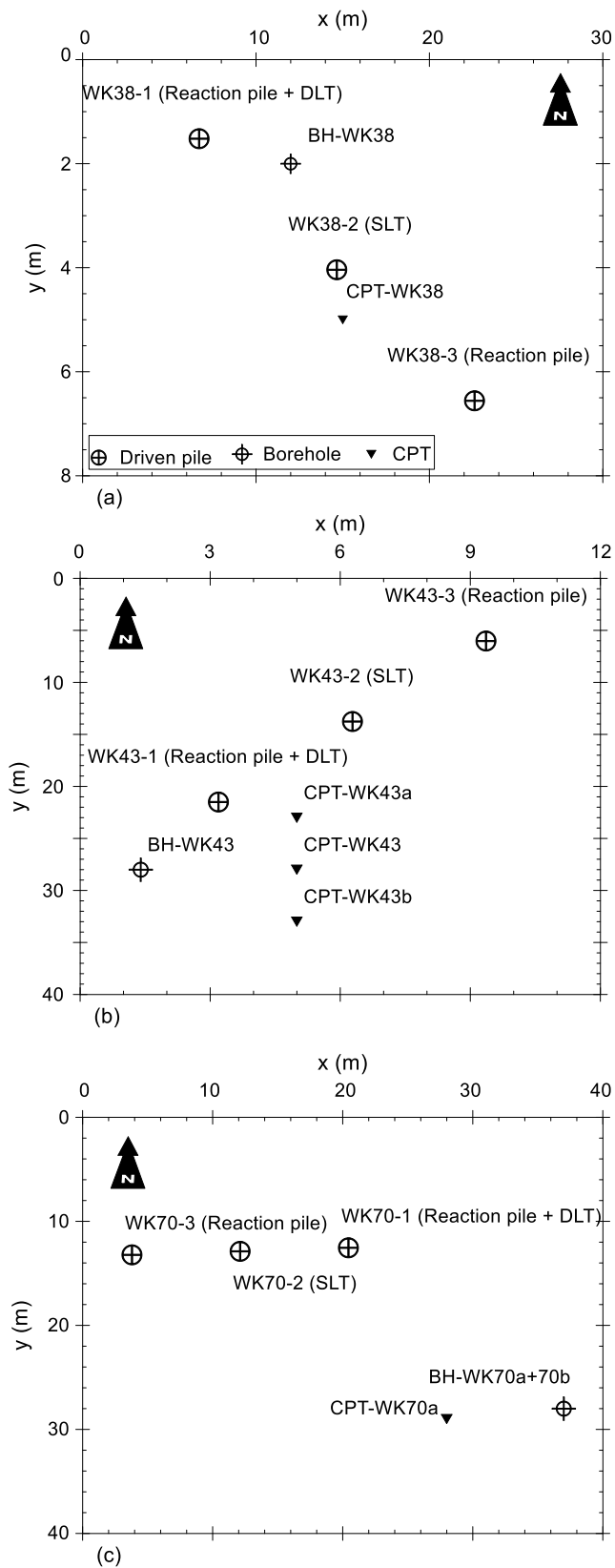


Figure 1 Plan showing relative layout of test piles, boreholes and cone penetration tests at each pre-construction test location (a) WK38 (b) WK43 (c) WK70 Note: each plan based on arbitrary site datum position

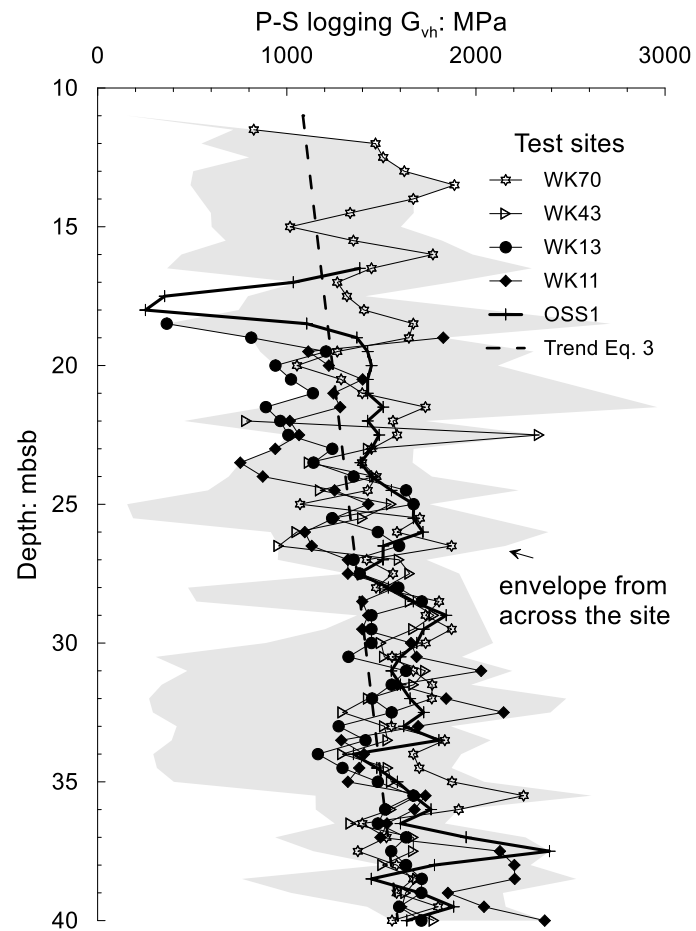


Figure 2 Shear modulus,  $G_{vh}$  in chalk from suspension P-S logging at the test sites (mbsb=metres below sea bed)

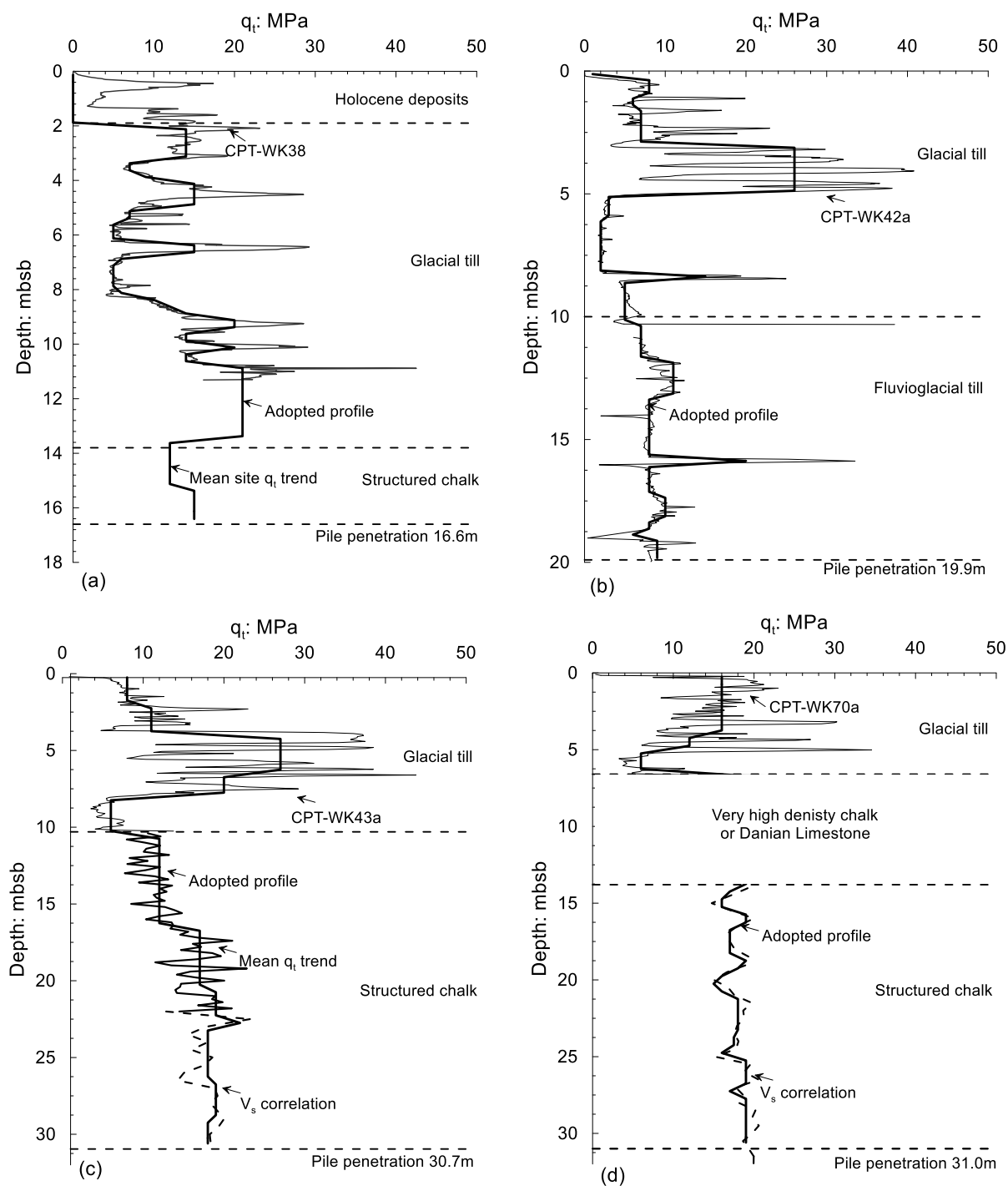


Figure 3 Site profiles at test sites (a) WK38 (b) WK42 (c) WK43 (d) WK70

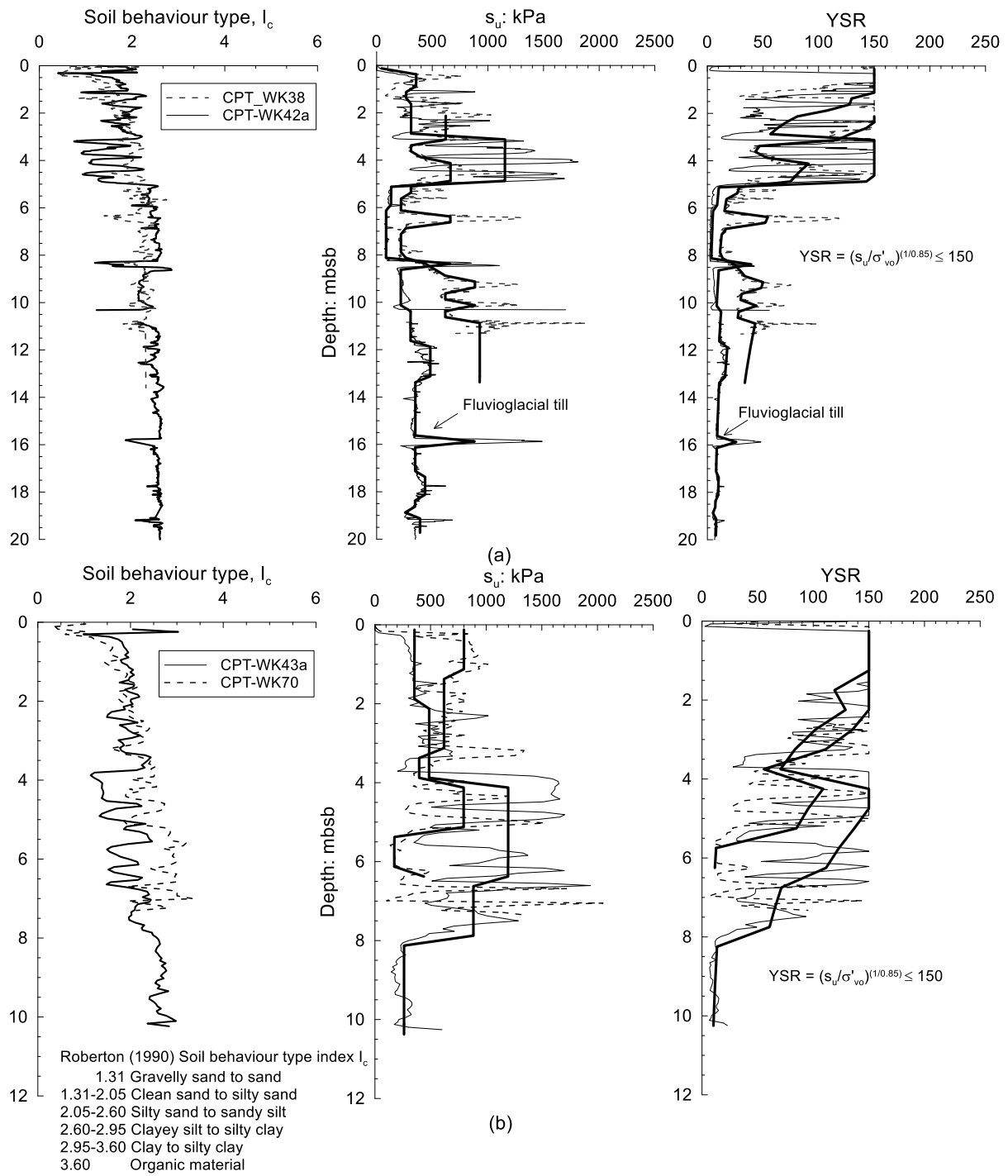


Figure 4 Profiles of soil behaviour type index,  $I_c$  (Robertson, 1990), undrained shear strength,  $s_u$ , calculated from the CPT cone resistance assuming clay behaviour and an  $N_{sk}$  factor of 22.5 and Yield Stress Ratio at (a) WK38 and WK42 (b) WK43 and WK70



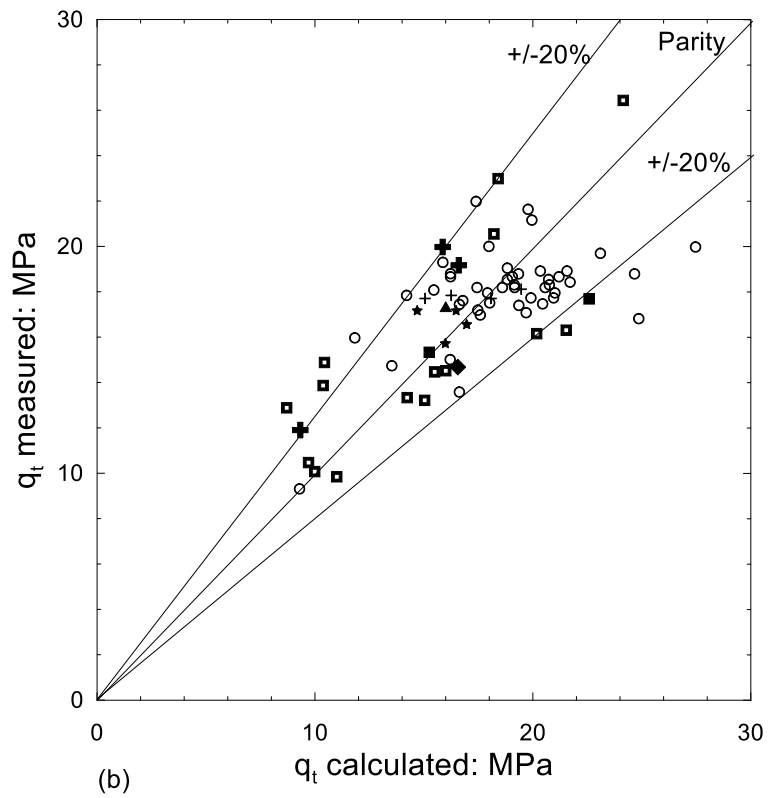
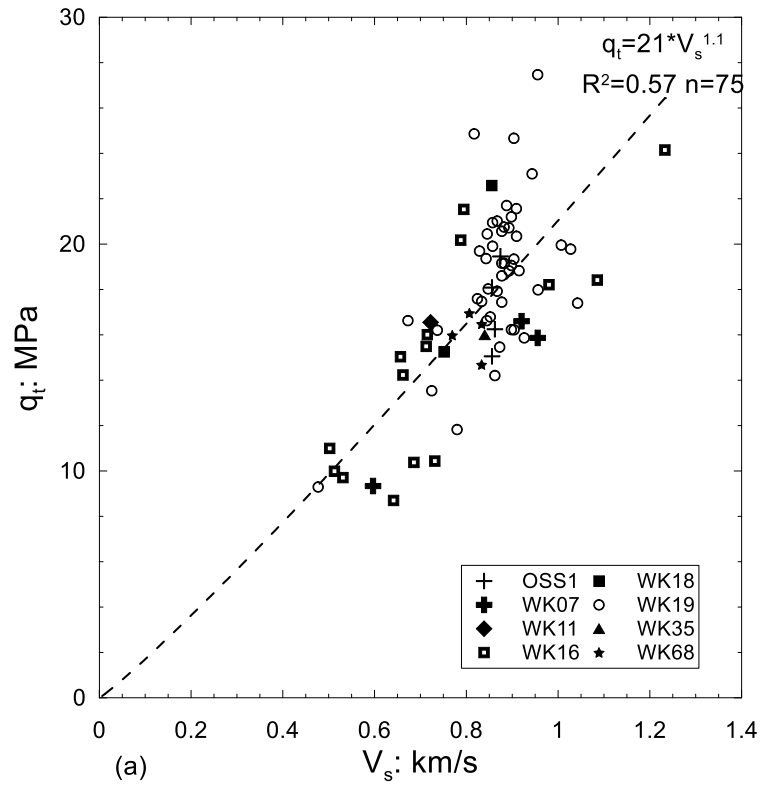


Figure 5 Correlation between cone resistances and shear wave velocity in chalk developed from the results at eight WK test locations (a) cone resistance,  $q_t$  versus shear wave velocity  $V_s$  (b) measured versus calculated  $q_t$

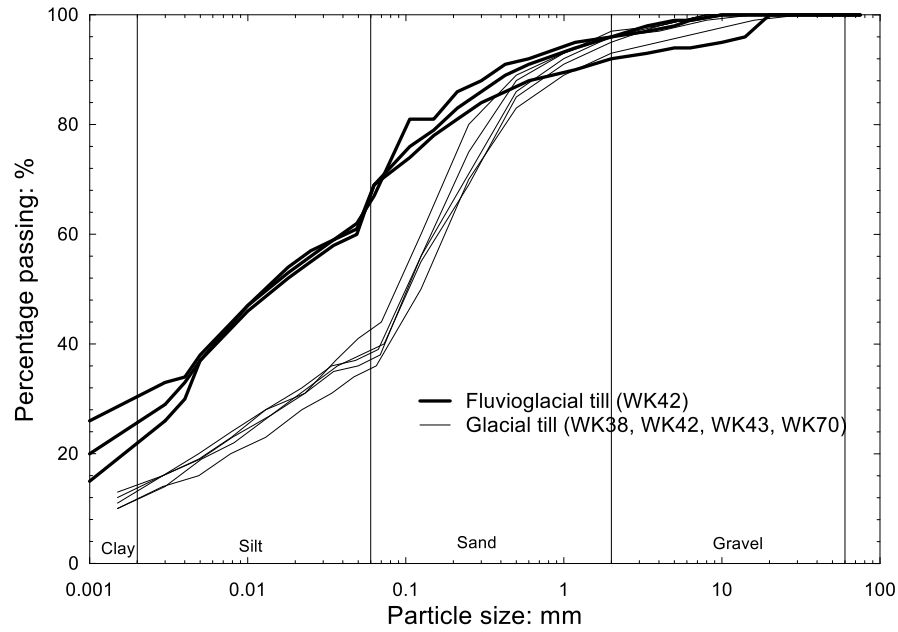


Figure 6 Particle size distributions in fluvioglacial and glacial till

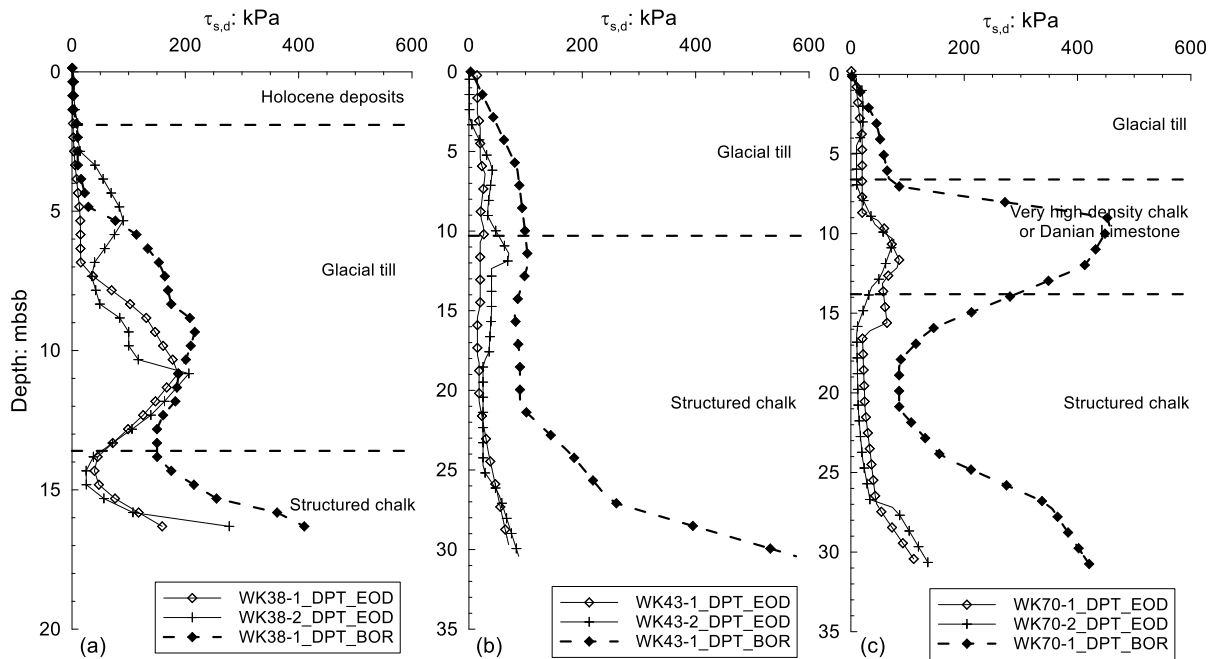
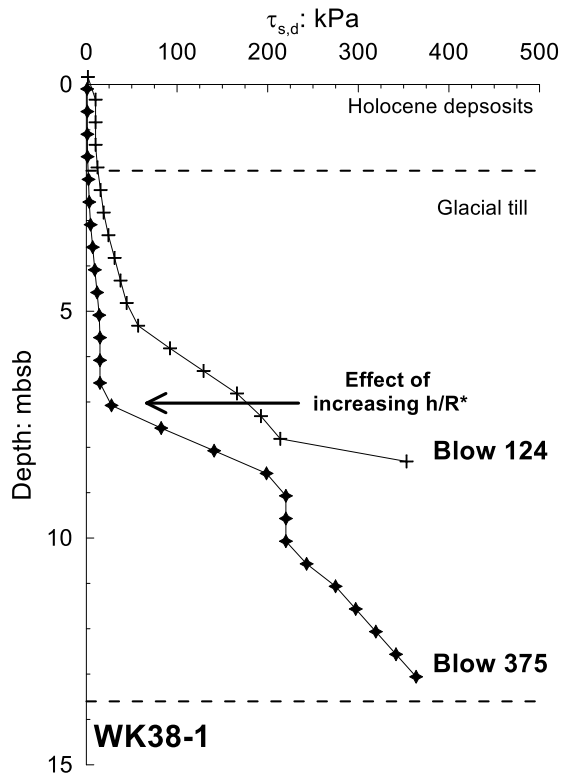
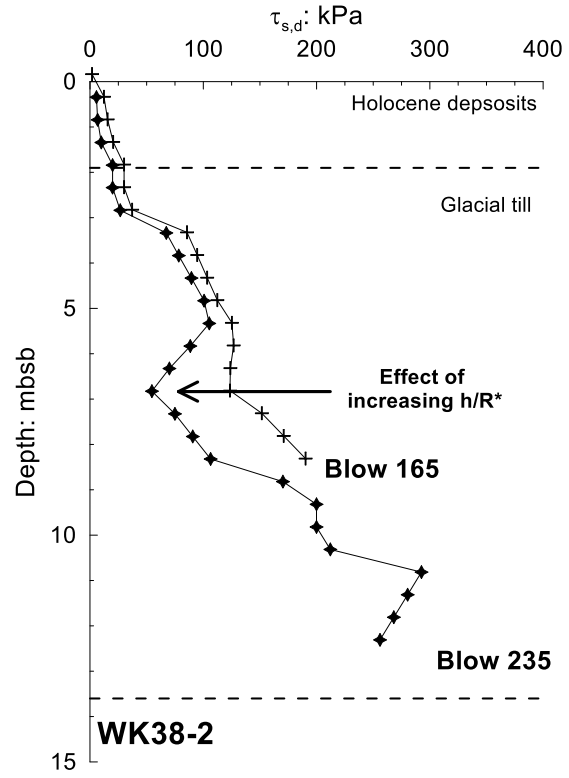


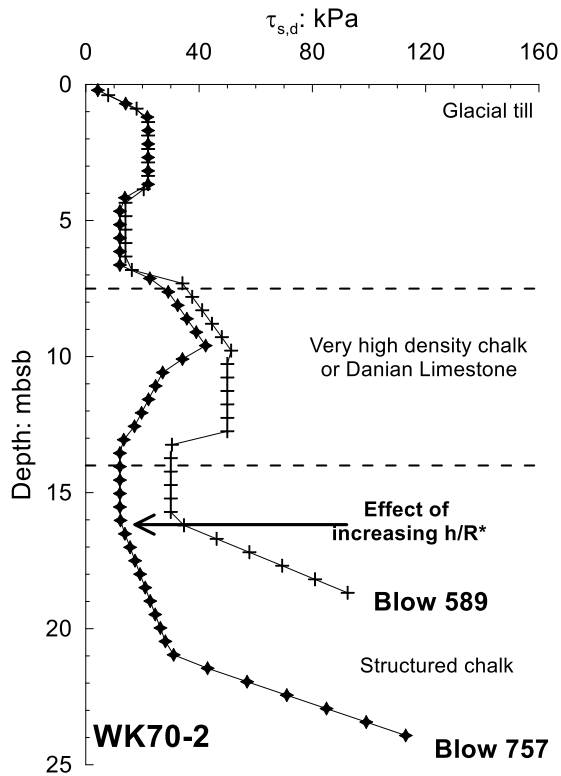
Figure 7 Compressive shaft resistance back analysed using IMPACT at end of driving and beginning of restrike (a) WK38 (b) WK43 (c) WK70



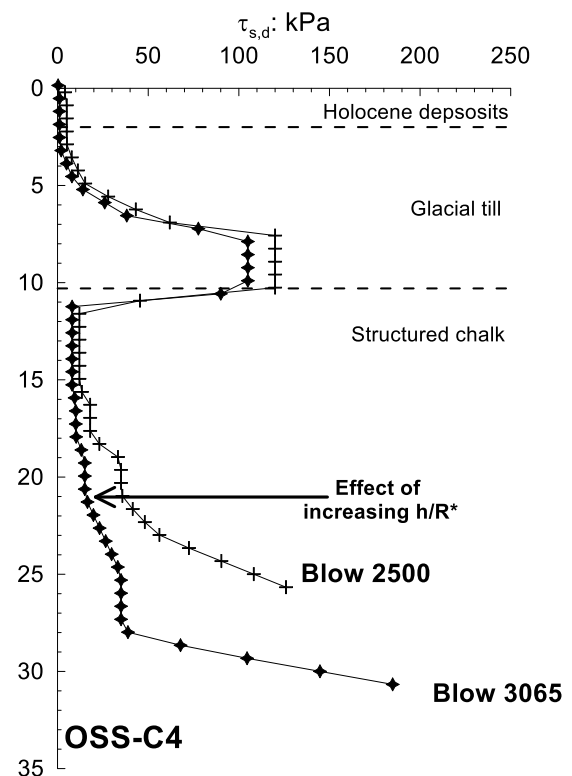
(a)



(b)

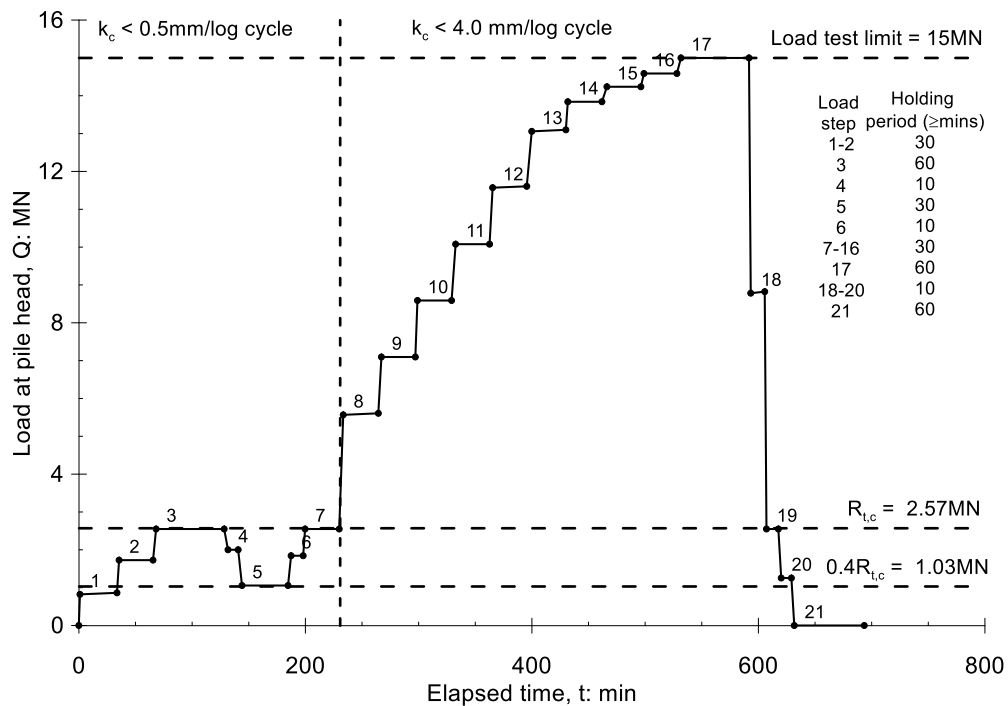
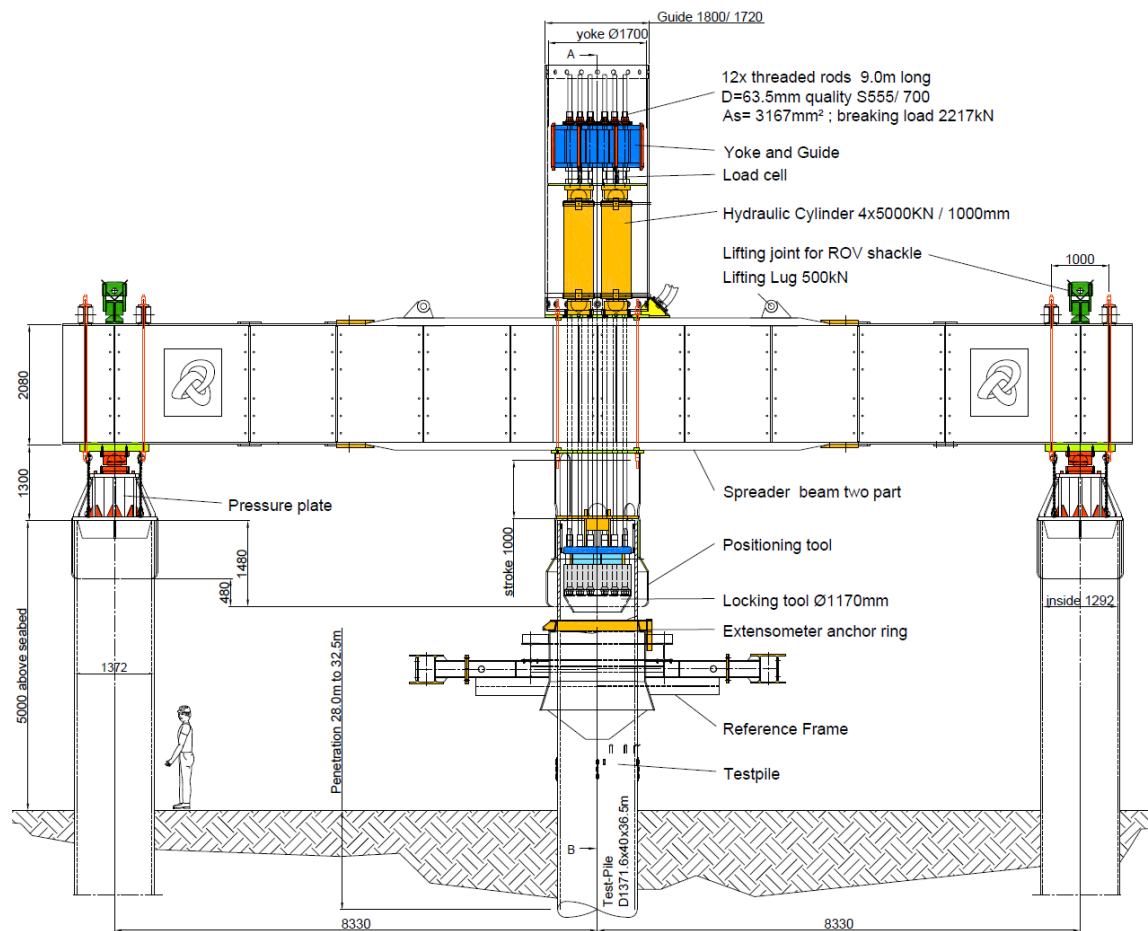


(c)



(d)

Figure 8 Illustration of dependence of compressive shaft resistance on  $h/R^*$  (a) mid driving blows during installation of WK38-1 (b) mid driving blows during installation of WK38-2 (c) mid driving blows during installation of WK70-2 (d) mid driving blows during installation of OSS-C4



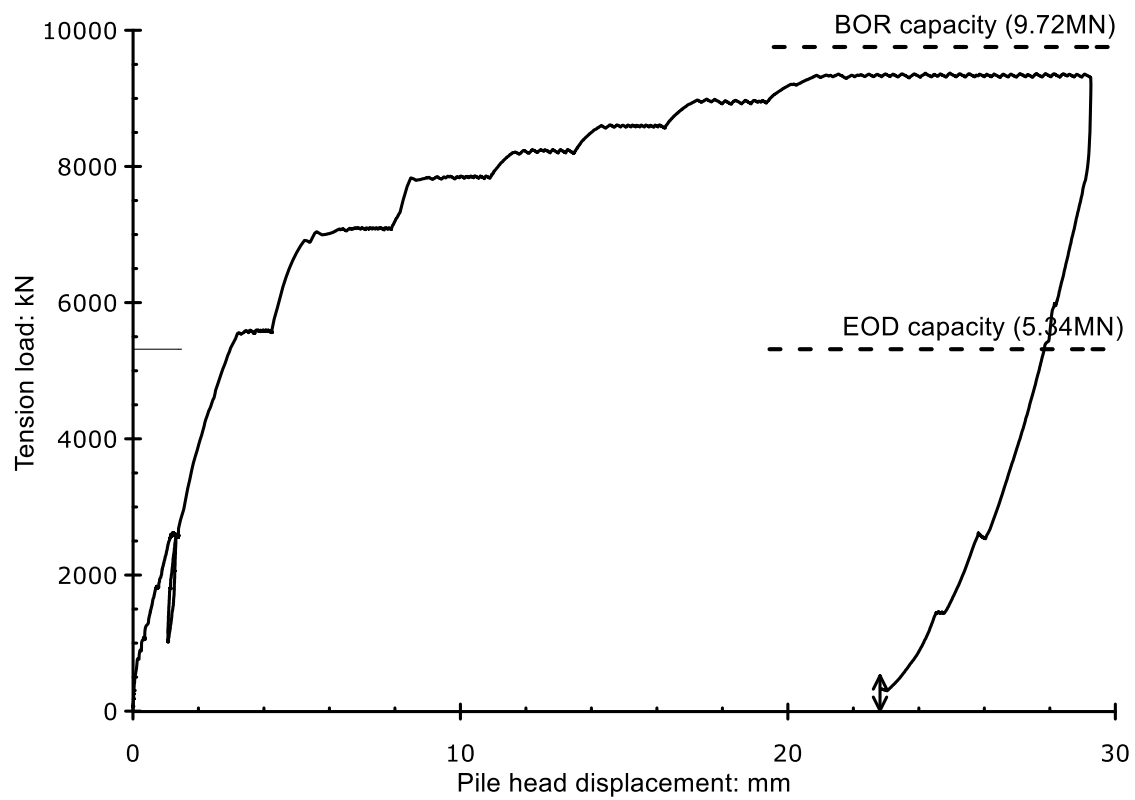


Figure 11 Load – displacement behaviour during static axial tension test WK38-2\_SLT\_108

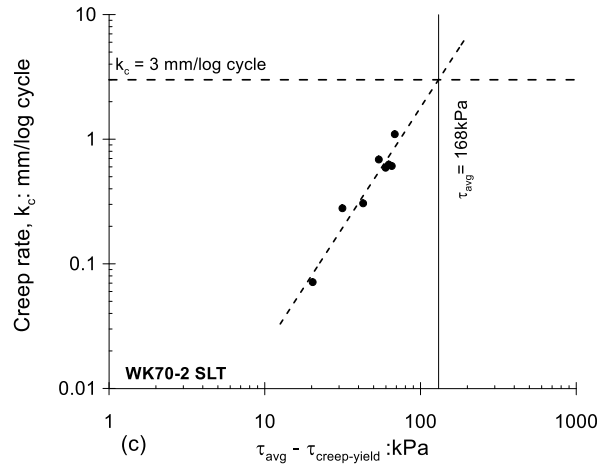
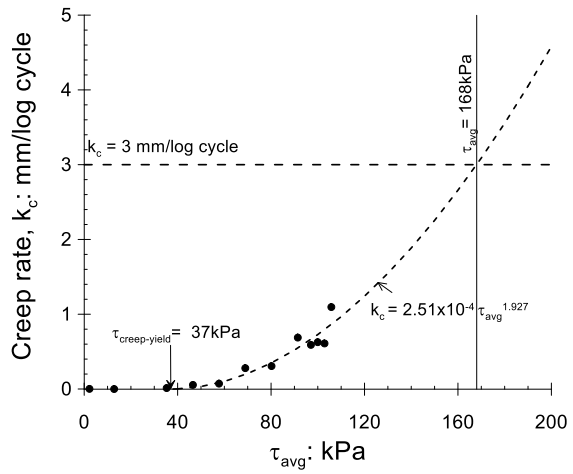
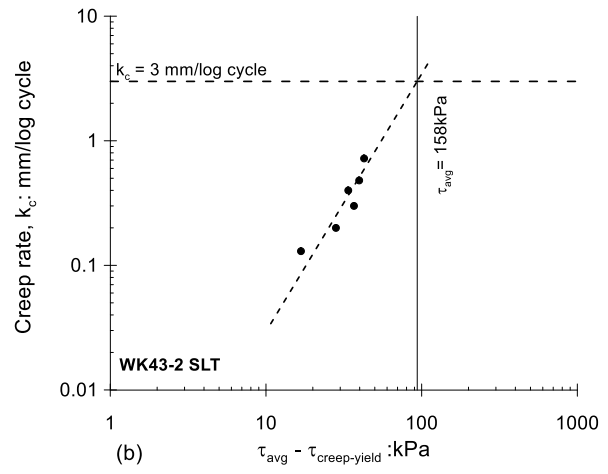
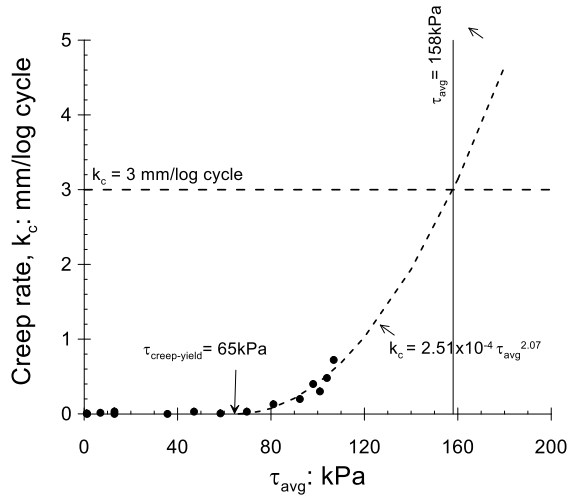
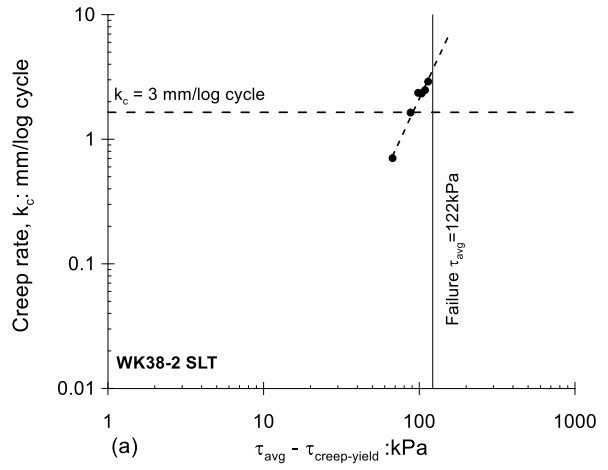
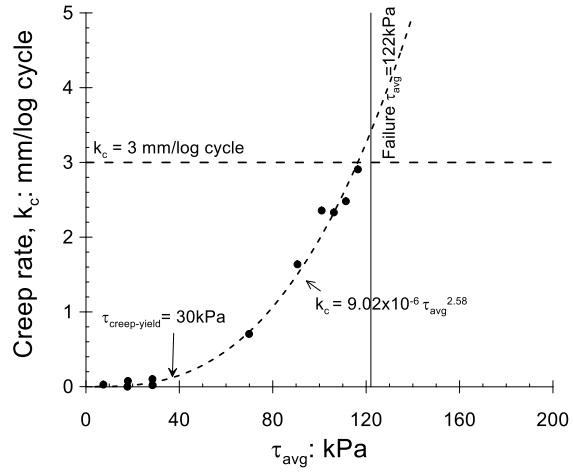


Figure 12 Extrapolation of creep rates to failure (a) WK38-2 (b) WK43-2 (c) WK70-2.  $\tau_{\text{avg}} - \tau_{\text{creep-yield}}$  is limit below which the creep rates were negligible

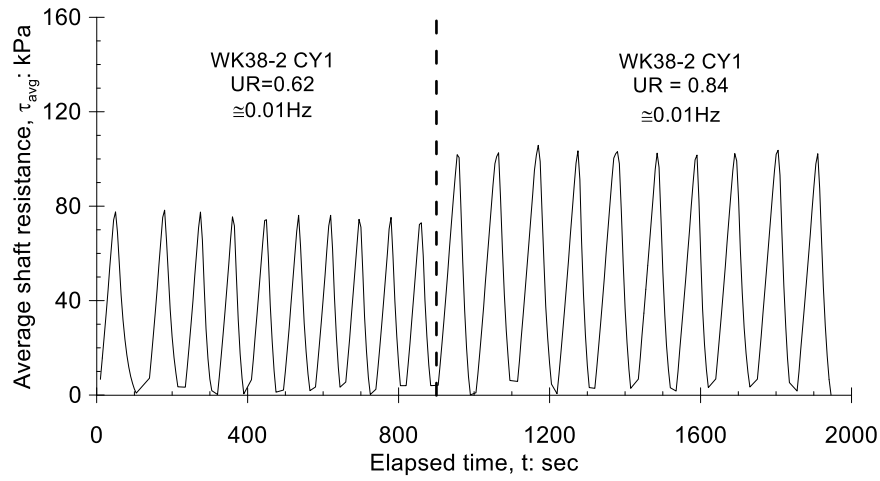


Figure 13 Average shaft resistance mobilised during WK38-2\_CYC\_108 versus time

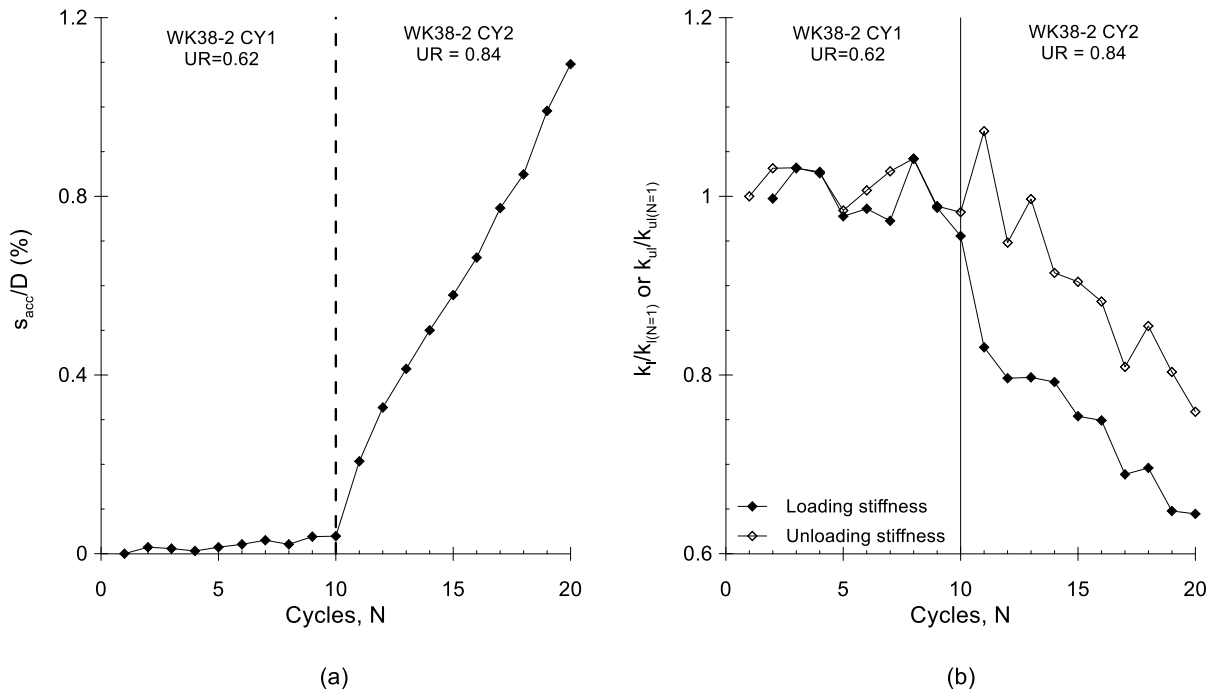


Figure 14 WK38-2\_CYC\_108 (a) permanent cyclic displacements normalised by pile diameter (b) cyclic loading and unloading stiffness

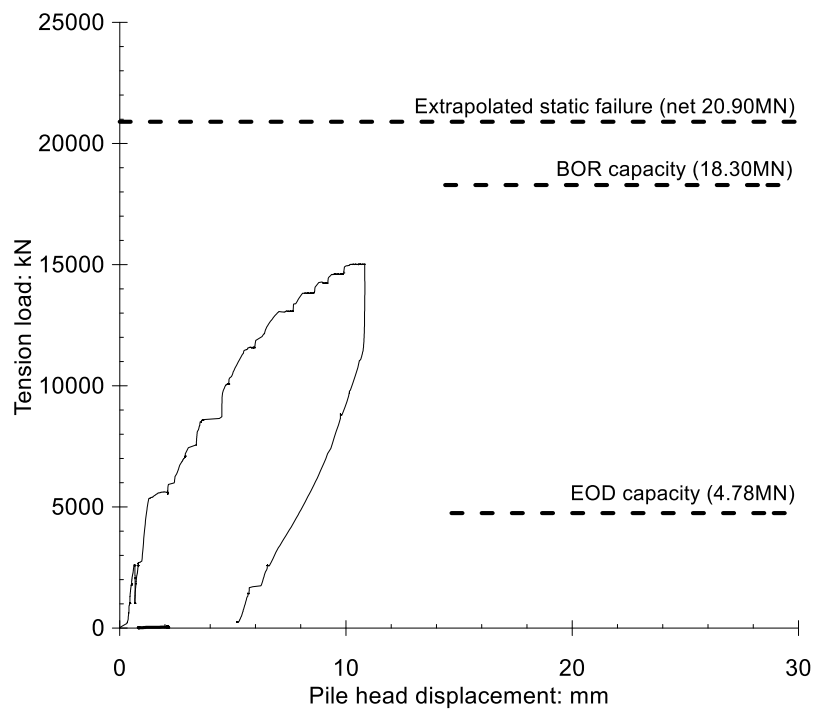


Figure 15 Load – displacement behaviour and extrapolated failure load during static axial tension test on WK43-2

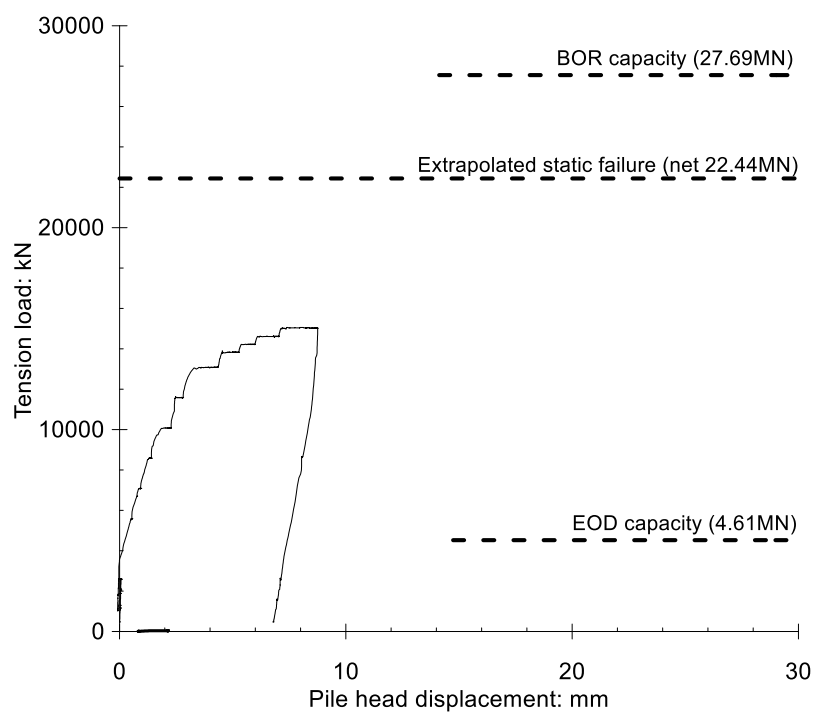


Figure 16 Load – displacement behaviour and extrapolated failure load during static axial tension test on WK70-2



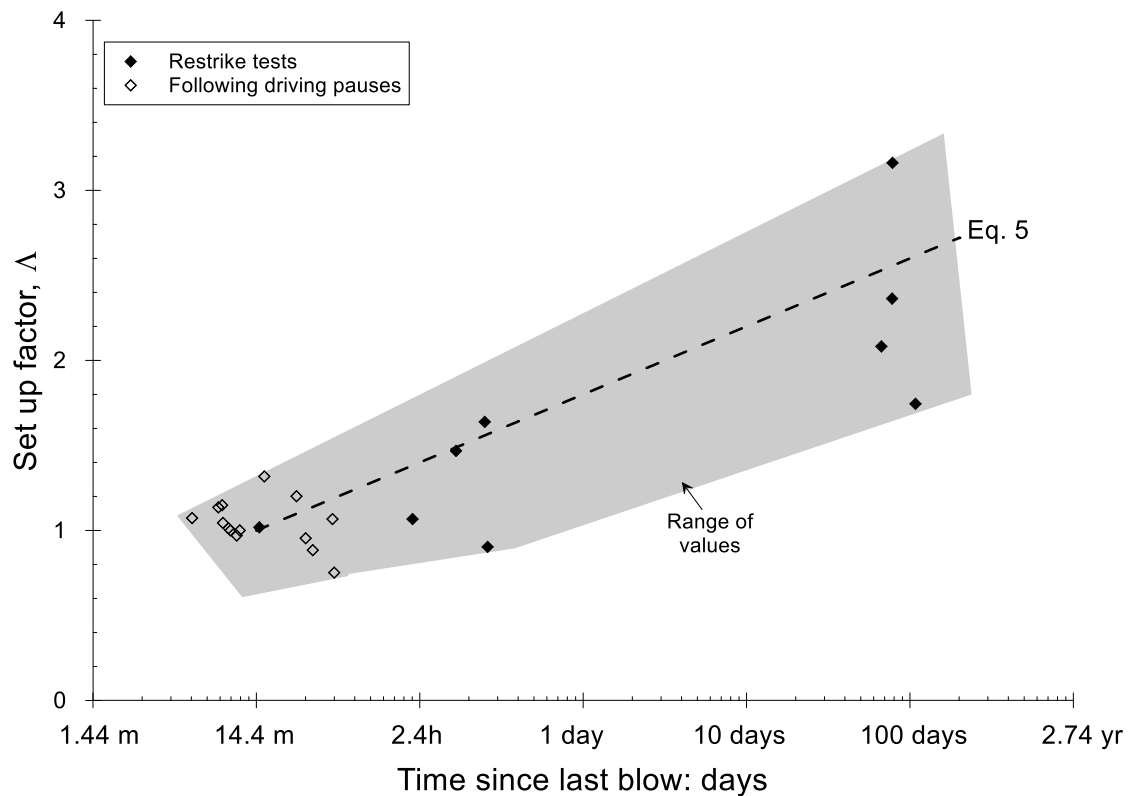


Figure 17 Set-up trends in glacial till from dynamic restrike tests and from blows following driving pauses with semi- logarithmic capacity increase trend without apparent asymptotic value over monitoring period

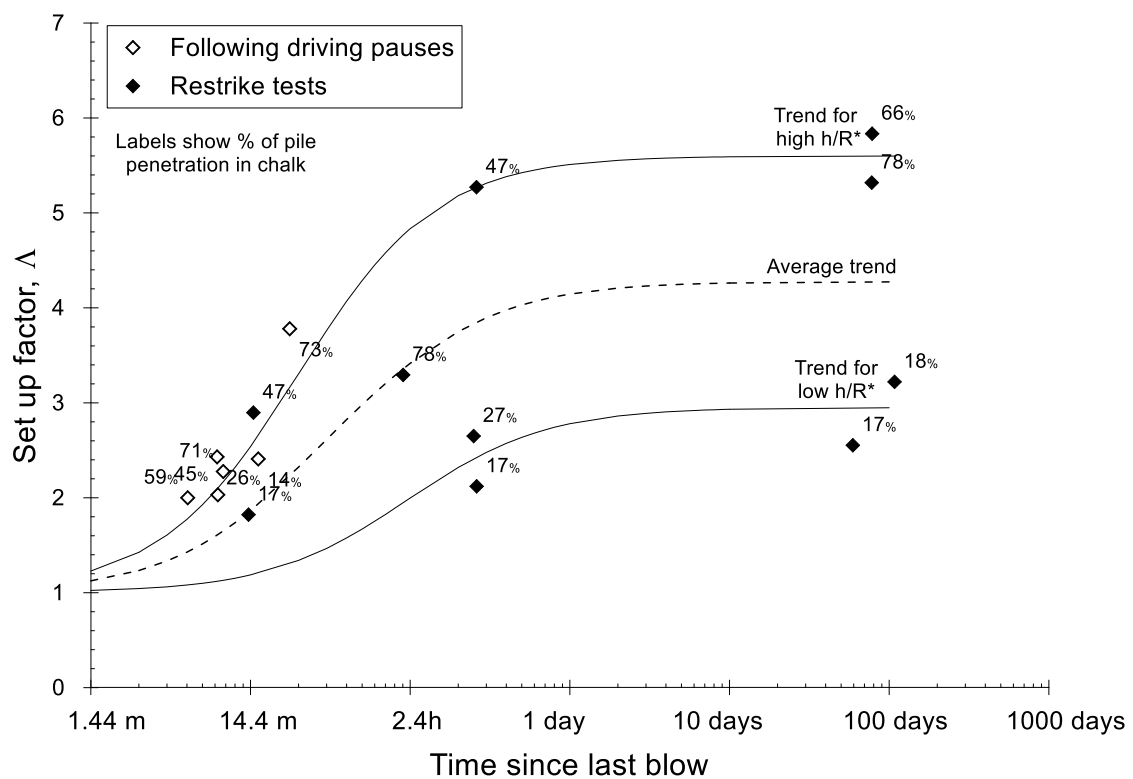


Figure 18 Set-up factors in chalk from dynamic restrike tests and from blows following driving pauses with interpreted trends for high and low  $h/R^*$  values

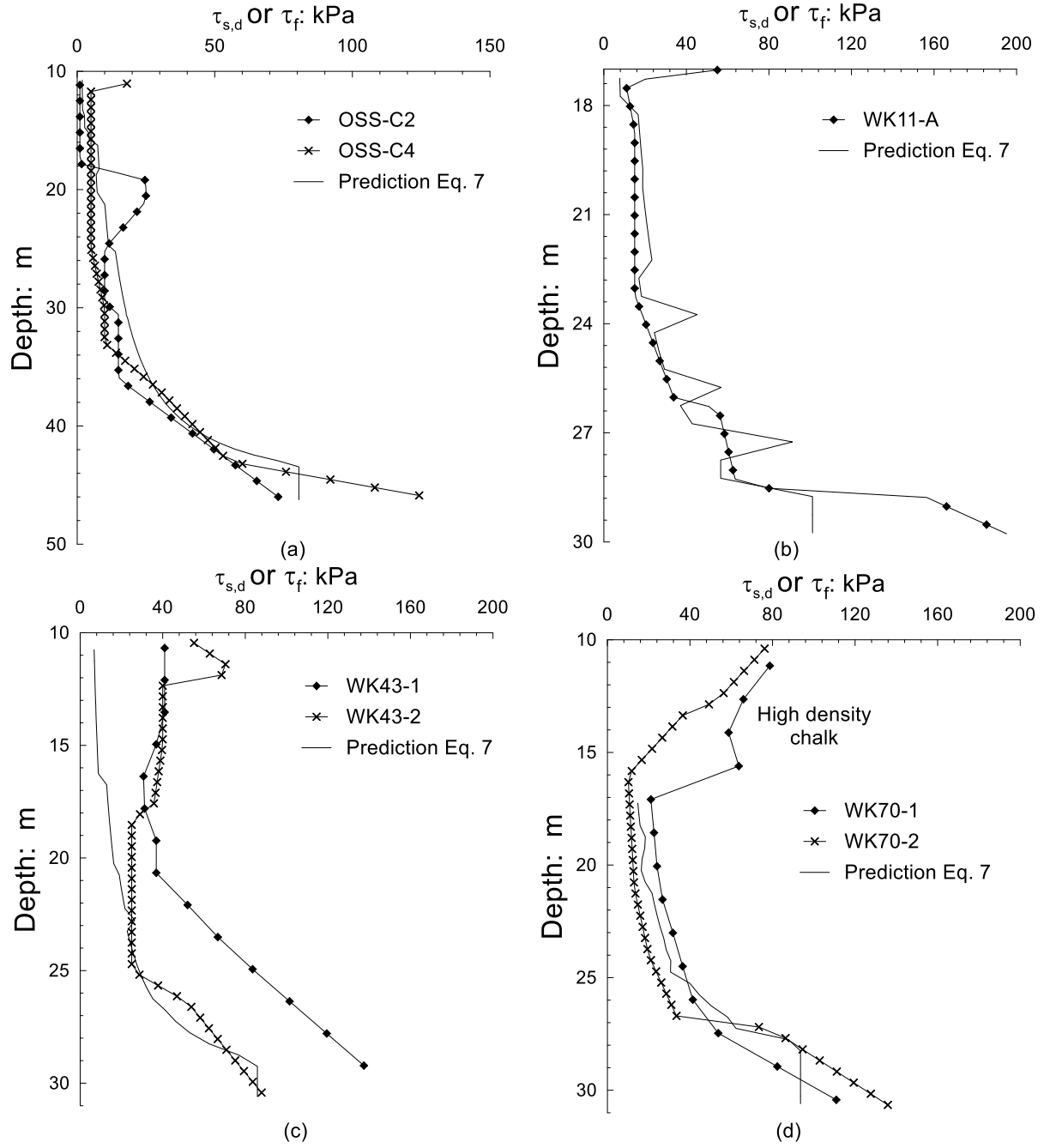


Figure 19 Examples of shear stress profiles at EOD interpreted from signal matching; profiles predicted using Eq. 7 and Eq. 2

## TABLES

Table 1 Details of the test sites, pile diameters and pile penetrations

Test site	Testing stage	$t_w$ (mm)	D (m)	Length of penetration, $L_p$ (m)					
				Total	Holocene	Glacial till	Fluvioglacial till	Chalk	CPT
WK38	Pre-construction	40	1.37	16.6	1.9	11.7	-	3.0	11.2
WK43	Pre-construction	40	1.37	30.7	-	10.3	-	20.4	11.0
WK70	Pre-construction	40	1.37	31.0	-	6.6 <sup>2</sup>	-	24.2	7.4
OSS	Production	60	3.67	46.3	2.0	8.3	-	36.0	35.7 <sup>1</sup>
WK08	Production	40.5	3.67	27.9	4.1	9.5	9.5	4.8	49.3
WK11	Production	40.5	2.70	31.1	4.5	12.0	-	14.6	33.3
WK13	Production	40.5	2.70	25.8	3.0	15.9	-	6.9	24.2
WK42	Production	40.5	2.70	19.9	0.1	9.9	9.2	0.7	50.4

1. Penetration of cone penetration test below seabed level

2. Re-interpretation of SI results indicates glacial till to 7.5m, underlain by Danian Limestone between 7.5 and 14m which is in turn underlain by L-M density chalk

Table 2: Index properties from the 8 test sites during the pre-construction and production piling stage

Parameter	Glacial till			Fluviogalcial till			Chalk		
	n	Mean	StDev	n	Mean	StDev	N	Mean	StDev
Water content, $w_c$ (%)	173	12.8	3.8	6	13.4	2.1	149	28.4	4.7
Saturated water content, $w_{sat}$ (%)	-	-	-	-	-	-	128	28.9	4.2
Liquid limit, $w_l$ (%)	58	21.5	4.5	5	20.8	3.6	-	-	-
Plastic limit, $w_{pl}$ (%)	58	12.7	1.7	5	12.6	1.3	-	-	-
Plasticity index, $I_p$ (%)	58	8.8	3.4	5	8.1	2.0	-	-	-
Bulk density, $\gamma_{bulk}$ (Mg/m <sup>3</sup> )	30	2.2	0.2	3	2.2	0.1	143	1.95	0.1
Dry density, $\gamma_d$ (Mg/m <sup>3</sup> )	30	1.9	0.2	-	-	-	-	-	-
Specific gravity, $G_s$	46	2.69	0.01	4	2.69	0.01	23	2.70	0.02
Intact dry density, IDD (Mg/m <sup>3</sup> )	-	-	-	-	-	-	143	1.52	0.1
UCS, $q_u$ (MPa)	-	-	-	-	-	-	55	0.39	0.24
Calcium carbonate (%)	-	-	-	-	-	-	30	93.2	9.4

Table 3 Summary of pile test codes and test histories during test campaigns

Test pile	Test code <sup>1</sup>	Pile age		Test type
		Days	mins	
WK38-1	WK38-1_DPT_EOD	0	0	Dynamic test end of driving
	WK38-1_DPT_BOR	108	278	Dynamic test beginning of restrike
WK38-2	WK38-2_DPT_EOD	0	0	Dynamic test end of driving
	WK38-2_SLT_108	108	-	Static test on aged pile
	WK38-2_CYC_108	108	-	Post static failure cyclic test
WK43-1	WK43-1_DPT_EOD	0	0	Dynamic test end of driving
	WK43-1_DPT_BOR	78	335	Dynamic test beginning of restrike
WK43-2	WK43-2_DPT_EOD	0	0	Dynamic test end of driving
	WK43-2_SLT_78	78	-	Static test on aged pile
WK70-1	WK70-1_DPT_EOD	0	0	Dynamic test end of driving
	WK70-1_DPT_BOR	77	989	Dynamic test beginning of restrike
WK70-2	WK70-2_DPT_EOD	0	0	Dynamic test end of driving
	WK70-2_SLT_77	77	-	Static test on aged pile
OSS-C2	OSS-C2_DPT_EOD	0	0	Dynamic test end of driving
	OSS-C2_DPT_BOR	0	240	Dynamic test beginning of restrike
OSS-C4	OSS-C4_DPT_EOD	0	0	Dynamic test end of driving
	OSS-C4_DPT_BOR	0	130	Dynamic test beginning of restrike
WK08-A	WK08-A_DPT_EOD	0	0	Dynamic test end of driving
	WK08-A_DPT_BOR1	0	14	Dynamic test beginning of restrike
	WK08-A_DPT_BOR2	0	376	Dynamic test beginning of restrike
	WK08-A_DPT_BOR3	59	230	Dynamic test beginning of restrike
WK11-A	WK11-A_DPT_EOD	0	0	Dynamic test end of driving
	WK11-A_DPT_BOR1	0	15	Dynamic test beginning of restrike
	WK11-A_DPT_BOR2	0	375	Dynamic test beginning of restrike
WK13-A1	WK13-A_DPT_EOD	0	0	Dynamic test end of driving
	WK13-A_DPT_BOR	0	360	Dynamic test beginning of restrike
WK42-B	WK42-B_DPT_EOD	0	0	Dynamic test end of driving
	WK42-B_DPT_BOR	67	-	Dynamic test beginning of restrike

1. The test code nomenclature gives the pile name (e.g. WK38-1), the type of test (DPT = dynamic pile test, SLT = static pile test, CYC = cyclic pile test) and the time of the test (EOD or Beginning of Restrike (BOR) for dynamic tests and number of days for the static tests).

Table 4: Pile shaft resistances at the end of driving and beginning of restrike for all twelve tests

Test pile	End of driving <sup>1</sup>			Beginning of restrike <sup>2</sup>		
	$\tau_{avg}^3$ (kPa)	$\tau_{till}$ (kPa)	$\tau_{chlk}$ (kPa)	$\tau_{avg}^3$ (kPa)	$\tau_{till}$ (kPa)	$\tau_{chlk}$ (kPa)
WK38-1	67	59	88	136	103	284
WK38-2	75	66	98	-	-	-
WK43-1	26	19	30	139	61	176
WK43-2	36	21	38	-	-	-
WK70-1	40	16	48	207	39	254
WK70-2	35	14	40	-	-	-
OSS-C2	24	27	17	78	39	89
OSS-C4	29	45	21	68	48	73
WK08-A	60	36	123	93	42	225
				115	59	247
				141	76	315
WK11-A	30	22	42	65	22	122
				105	19	221
WK13-A	67	48	53	103	79	141
WK42-B	86	73	-	175	152	-

1. Final blow at the end of driving  
 2. First full energy blow during a restrike test  
 3. Average shaft resistance in the glacial till and chalk

Table 5: Summary of pile capacities from dynamic and static pre-construction pile tests and proportions in glacial till and chalk

Overall shaft capacity $Q_s$ (MN)					
Site	BOR <sup>1</sup>	SLT (net) <sup>2</sup>	BOR/Static	%Glacial till	%Chalk
WK38	9.72	8.80	1.10	69	31
WK43	18.30	20.90 <sup>3</sup>	0.88	14	86
WK70	27.69	22.44 <sup>3</sup>	1.23	4	96

1. From IMPACT analysis of re-strike data BOR=Beginning of restrike
2. SLT (net) = static capacity corrected for soil/chalk and steel weight
3. Based on extrapolation of creep rates to  $k_c=3\text{mm/log cycle}$

Table 6: Extrapolation of shaft loads to ultimate conditions using available methods

Site	Extrapolated overall net shaft load $Q_s$ (MN)				Measured or adopted value (MN)
	<a href="#">Chin (1970, 1971)</a>	<a href="#">Decourt (1999)</a>	<a href="#">Brinch Hansen (1963)</a>	Creep rate (3mm/log cycle)	
WK38	10.05	14.00	10.71	8.40	8.80 <sup>1</sup>
WK43	21.74	21.98	17.25	20.90	20.90
WK70	17.10	18.14	16.70	22.44	22.44

1. Measured value for full failure test

Table 7 Static tension failure loads and pile capacity predictions for offshore pile tests at Wikingen

	WK38-2	WK43-2	WK70-2
Time after driving (days)	108	78	77
Tensile failure load, $Q_t$ (MN)	9.33	21.77 <sup>1</sup>	23.31 <sup>1</sup>
Pile and chalk self-weight (MN)	0.53	0.87	0.87
Average tensile shaft resistance, $\tau_{avg}$ (kPa)	122	158 <sup>1</sup>	168 <sup>1</sup>
Compressive EOD shaft load on Pile -2 (MN)	5.34	4.78	4.61
Compressive BOR shaft load on Pile -1 (MN)	9.72	18.30	27.69
Global set up factor, $\Lambda$ (static/EOD)	1.65	4.37	4.86

1. Based on extrapolation of creep rates to  $k_c=3\text{mm/log cycle}$

Table 8: Summary of operational pauses in pile driving and interpreted shaft stresses before and following a pause

Test pile	Duration (mins)	Beginning of Pause		End of Pause	
		$\tau_{till}$ (kPa)	$\tau_{chlk}$ (kPa)	$\tau_{till}$ (kPa)	$\tau_{chlk}$ (kPa)
OSS-C2	10	26.4	41.8	26	111
OSS-C4	10	28.2	41.1	29	94
WK08-A	7	93.9	-	102	-
WK38-1	42	24.9	-	27	-
	29	87.2	-	83	-
WK38-2	43	34.9	-	26	-
	11	74.2	-	72	-
	32	88.7	-	78	-
WK42	11	24.5	-	24	-
WK43-1	16	13.4	99.5	18	240
	6	2.3	51.4	2	106
WK43-2	9	35.3	78.5	41	215
WK70-1	8	26.0	95.3	30	194
WK70-2	9	27.5	54.0	29	118
WK70-2	25	16.4	31.1	20	120

1. Final blow before pause begins

2. First blow following pause

Table 9: Summary of static pile capacity predictions in the glacial till

Site	Shaft load $Q_s$ in glacial till layer (MN)						
	Measured <sup>1</sup>	ICP-05 sand <sup>2</sup>	API-2014 <sup>2</sup>	Fugro-96 <sup>2</sup>	NGI-05 <sup>2</sup>	UWA-13 <sup>2,3</sup>	ICP-05 clay <sup>2</sup>
WK38	6.07	2.29 (0.38)	9.21 (1.52) <sup>4</sup>	11.62 (1.91) <sup>4</sup>	9.52 (1.57) <sup>4</sup>	19.53 (3.22) <sup>4</sup>	12.39 (2.04) <sup>4</sup>
WK43	2.93	1.19 (0.41)	7.48 (2.56)	6.37 (2.18)	7.52 (2.57)	13.95 (4.77)	6.04 (2.07)
WK70	0.90	0.64 (0.72)	4.49 (5.00)	3.41 (3.80)	4.45 (4.94)	7.89 (8.79)	3.85 (4.29)

1. Proportion based on static values given in Table 5
2. Values in parentheses are ratios of calculated to measured capacity
3. Uses UWA-13 method with inclusion of angle of interface friction (Eq. 8)
4. Adopts ICP-05 calculation in top 2m of Holocene sand

Table 10: Summary of static pile capacity predictions in chalk

Long-term (>100 day) shaft load $Q_s$ in chalk layer (MN)			
Site	Measured <sup>1</sup>	CIRIA C574 <sup>2</sup>	Chalk ICP-18 <sup>2,3</sup>
WK38	2.73	0.27 (0.10)	3.31 (1.21)
WK43	17.97	1.76 (0.10)	14.23 (0.79)
WK70	21.54	4.83 <sup>4</sup> (0.22)	21.67 <sup>5</sup> (1.01)

1. Proportion based on static values given in Table 5
2. Calculation assumes  $\Delta r = 0.5 \mu m$  with  $G$  calculated from Eq. 3
3. Values in parentheses are ratios of calculated to measured capacity
4. Adopts 120kPa in high density chalk/Danian Limestone layer
5. Adopts  $q_t=50MPa$  in the high density chalk/Danian Limestone layer

## APPENDIX 1 TRIAXIAL BEHAVIOUR OF WIKINGER CHALK AND TILL

---

Appendix 1 provides illustrations of the behaviour seen in triaxial tests on high quality samples of chalk and till taken during the Wikingen windfarm site investigations.

### *Chalk*

The effective stress paths and stress-strain behaviour observed in CAU triaxial tests is shown on Figure 20 for intact samples of structureless, structured low and medium density chalk. Note that the externally measured strains are likely to be substantially higher than the local values due to compliance effects (see [Jardine \*et al.\*, 1985](#)). The overall behaviour is consistent with that reported in the literature for intact chalk (e.g. [Jardine \*et al.\*, 1985](#), [Addis and Jones, 1990](#), [Leddra \*et al.\*, 1993](#)). The low density samples are interpreted as showing peak values of  $36^\circ$  with  $c'$  of 150kPa. Cohesion appears to increase with IDD, consistent with these chalks possessing a more cemented fabric; peak  $\phi'$  in medium density samples was similar at  $36.4^\circ$ , however cohesion was closer to 200kPa.



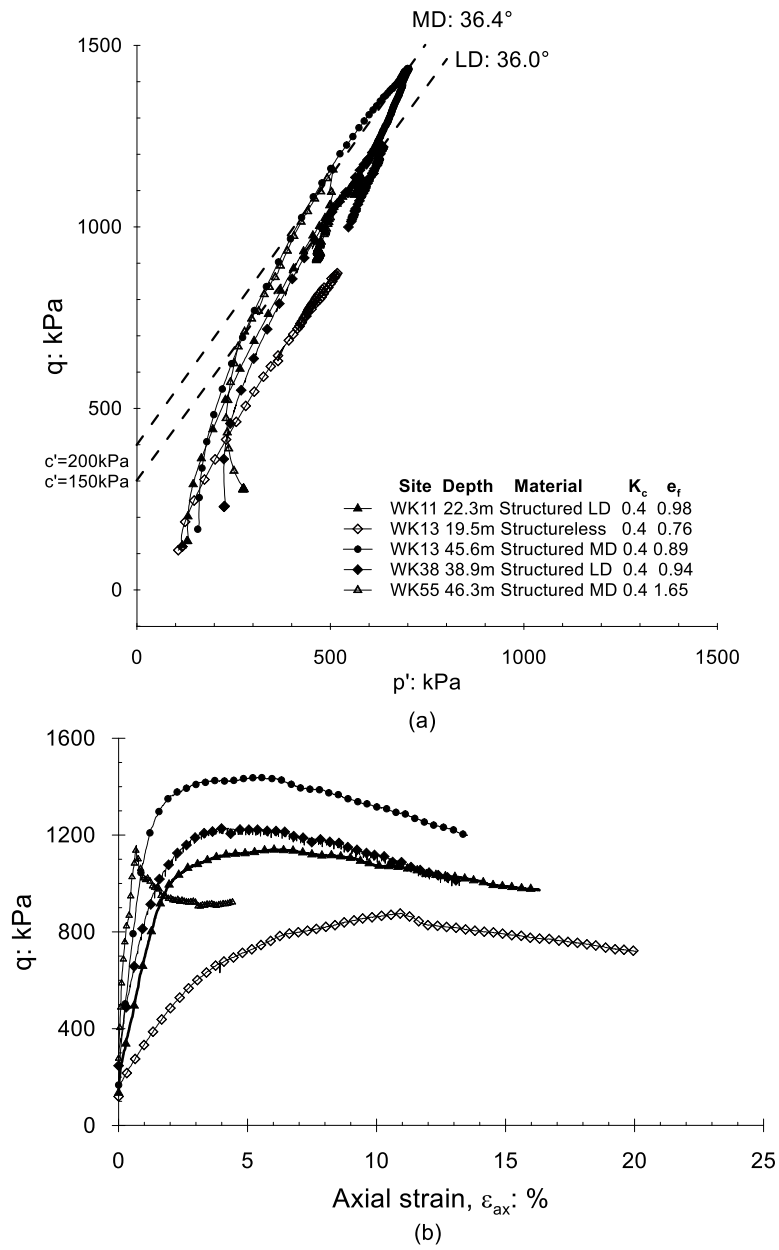


Figure 20: Triaxial tests on samples of intact structured and structureless chalk (a) effective stress paths (b) deviator stress versus axial strain (tests conducted by GEO)

## Glacial till

The undrained effective stress paths and stress-strain plots from typical CAU tests, conducted by GEO, on glacial till samples from the test sites are shown on Figure 21. The maximum  $s_u$  values found from CAU tests range from  $\approx 200$  to  $1000$  kPa. The specimens appear to reach critical state with  $M_{tc} = 1.44$  ( $\phi'_{cv} = 35.5^\circ$ ) with their end points falling on a unique line in specific volume - mean effective stress space, with slope  $\lambda = 0.07$  ( $C_c = 0.161$ ) and  $\Gamma$  at  $p' = 1$  kPa of  $1.68$ . The latter value of  $C_c$  is consistent with values reported by [Gens \(1982\)](#) on samples of Cromer till, by [Jardine \(1985\)](#) for Magnus till and by [Ushev \(2018\)](#) for Cowden till.

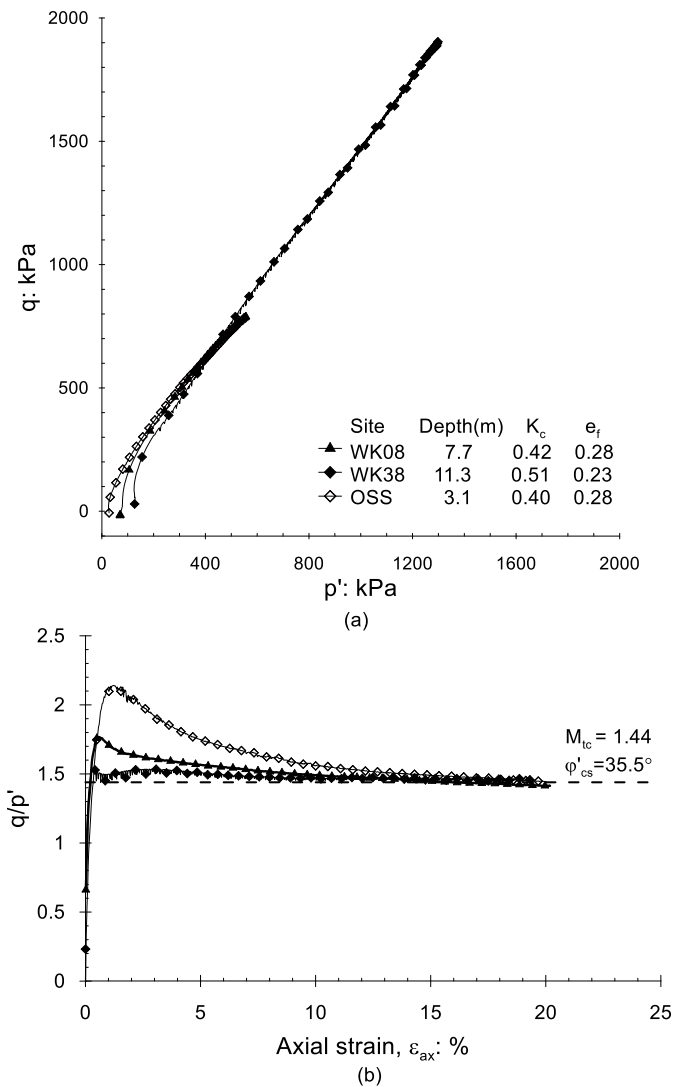


Figure 21: CAU triaxial tests on samples of glacial till (a) effective stress paths (b)  $q/p'$  versus axial strain (tests conducted by GEO)

## APPENDIX 2 ICP-05 CLAY METHOD PARAMETERS

---

The ICP-05 clay design procedure relies critically on establishing the profiles of YSR, defined as:

$$\text{YSR} = \frac{\sigma'_{vy}}{\sigma'_{v0}} \quad \text{Eq. 11}$$

here  $\sigma'_{v0}$  is the effective overburden pressure and  $\sigma'_{vy}$  is the effective vertical yield stress which can sometimes be obtained from oedometer tests, but may be difficult to resolve in tests on stiff glacial tills ([Lehane, 1992](#)). Estimates can also be made from the ratio  $s_u/\sigma'_{v0}$  which is often related to YSR using relationships such as the one given by [Jardine et al. \(2005\)](#):

$$\frac{s_u}{\sigma'_{v0}} = \left( \frac{s_u}{\sigma'_{v0}} \right)_{nc} \text{YSR}^{0.85} \quad \text{Eq. 12}$$

where  $(s_u/\sigma'_{v0})_{nc}$  is the value from CAU compression tests on  $K_0$  consolidated samples, which lies between 0.25 and 0.35 for a range of materials. The above relationship is only valid for low plasticity clays that fail in a ductile manner such as at Wikingen and a value of 0.3 is adopted.

Site-specific drained interface shear angles are also critical to any ICP-05 analyses undertaken in clay layers. The large strain interface shear behaviour was investigated by [Buckley \(2018\)](#) through ring shear interface tests in the Bishop ring shear apparatus at Imperial College ([Bishop et al., 1971](#)) using interfaces with similar roughnesses to that of a driven pile ( $R_a=10\text{-}15\mu\text{m}$ ). Three tests were carried out in which the glacial till was first sieved to remove particles  $>425\mu\text{m}$  ( $\approx 10\text{-}14\%$ ). Sieving is necessary as coarse particles can affect the results due to the limited specimen thickness, but could lead to results that are not fully representative of *in situ* behaviour. The remaining material was then remoulded and placed in two layers, as close to natural moisture content as practicable. The test procedure followed the recommendations of [Jardine et al. \(2005\)](#).

The results, shown on Figure 22, indicate that in all three cases  $\delta'_{\text{peak}}$  and  $\delta'_{\text{ult}}$  were reached at displacements of  $<2\text{mm}$  and  $<10\text{mm}$  respectively. When examined upon completion of the test, all three samples had adhered to the interface. There was no evidence of polishing or formation of a shear surface at the interface. The values of  $\delta'_{\text{ult}}$  are  $<0.5^\circ$  lower than the  $\delta'_{\text{peak}}$  values. While [Lehane and Jardine \(1994\)](#)

report lower ultimate angles (22-24°) for a glacial clay at Cowden, where the fines content was significantly higher (30% clay and 50% silt), [Ushev \(2018\)](#) found higher angles for Cowden till and [Jardine \(1985\)](#) reported higher values for Magnus till. [Iverson \*et al.\* \(1998\)](#) demonstrated the tendency for ultimate friction angles in glacial till to reduce with increasing clay content.

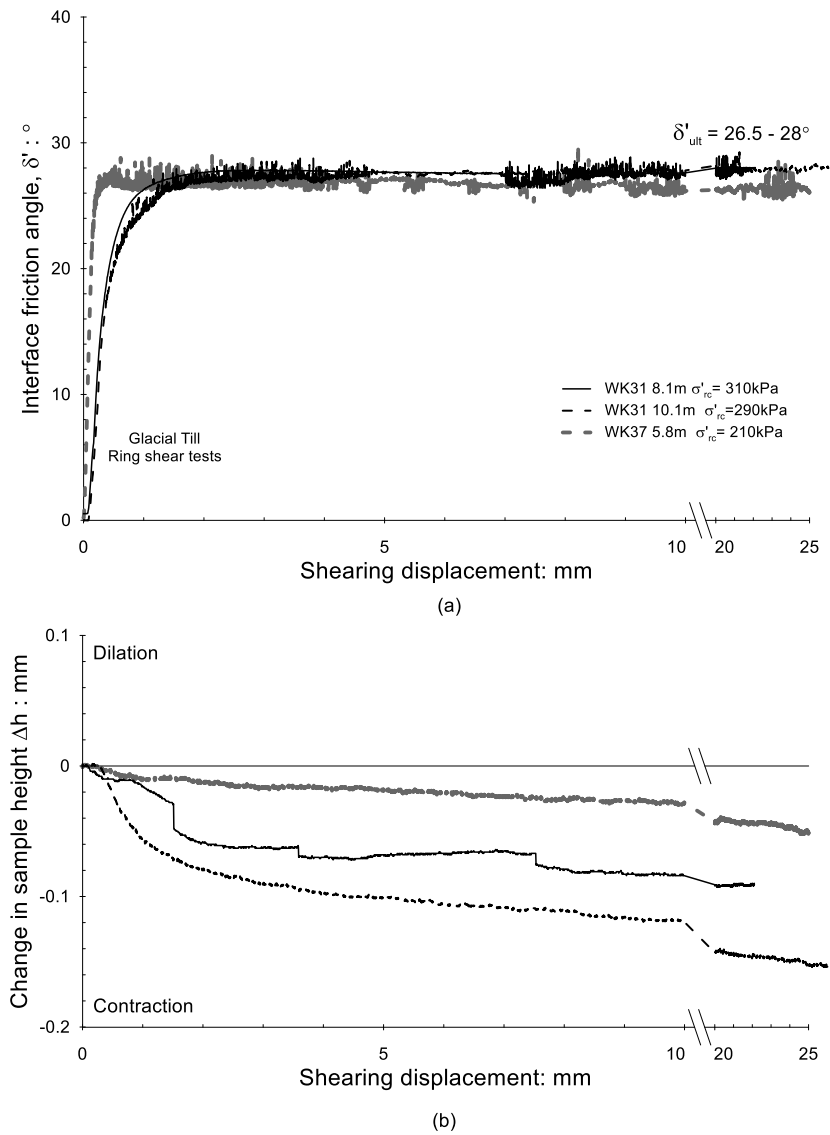


Figure 22: Ring shear tests on samples of glacial till conducted at Imperial College (a) interface friction angle versus displacement (b) change in sample thickness versus displacement ([Buckley, 2018](#))

## APPENDIX 3 SUMMARY OF DYNAMIC ANALYSES

---

The analyses of the Wiking dataset employed the IMPACT software ([Randolph, 2008](#)) adopting the [Randolph and Simons \(1986\)](#) soil model for the shaft and the [Deeks and Randolph \(1995\)](#) model at the toe, as summarised in Table 11 and by [Buckley \*et al.\* \(2017\)](#). In both models, the primary input parameters of shaft and base resistance, soil density and shear modulus are linked to measurable soil properties. The values of  $G$  were secant values,  $G_1$  degraded from the small strain,  $G_{\max}$  values to account indirectly for soil non-linearity, following [Alves \*et al.\* \(2009\)](#) and [Salgado \*et al.\* \(2015\)](#). In the Holocene and glacial till, the best matches were obtained taking  $G_1$  close to  $200\sigma'_{v0}$ , following the recommendations of [Lee \*et al.\* \(1988\)](#) for sandy soils, which resulted in  $G_1/G_{\max}$  ratios of  $<0.3$ . In the chalk, the trend with depth obtained from the P-S logging  $V_s$  measurements was used to estimate  $G_{\max}$  with depth (Eq. 3) which was then reduced to  $G_1=0.2G_{\max}$ . The same values of shear modulus were adopted for both EOD and BOR analyses. The viscosity parameters,  $\alpha_s$  and  $\beta_s$  along the shaft were calculated from the correlations given by [Loukidis \*et al.\* \(2008\)](#). For clays,  $\beta_s = \beta_b = 0.2$  and the value of  $\alpha_s$  at the shaft is given by:

$$\alpha_s = 1.65 - 0.75 \left( \frac{s_u}{p_a} \right) \quad \text{Eq. 13}$$

Where  $p_a$  is atmospheric pressure. For both the Holocene/till and the chalk,  $\beta_s$  was taken as 0.2, consistent with the recommendation of [Randolph \(2008\)](#). The adopted value of  $\alpha_s$  in the chalk was 1.1, taking  $s_u$  from remoulded samples to reflect the soft behaviour expected in the annulus of chalk putty close to the shaft. However, substitution of the intact strength for glacial till into Eq. 13 gives a negative value of  $\alpha_s$ , as the correlations were not developed for such high strength insensitive materials. While [Brown and Hyde \(2008\)](#) reported minimal rate dependence in Statnamic loading tests conducted in glacial tills where the *in situ* moisture content was close to the plastic limit, the Authors are not aware of any similar findings applying to such tills during fully dynamic driving. [Lehane and Jardine \(1994\)](#) showed that rate effects had a significant impact on axial installation resistance in Cowden glacial till, for which loading rate has also been found to have a considerable on lateral pile capacity ([McAdam \*et al.\*, 2018](#)). The  $\alpha_s$  value of 1.15 which gave the best quality signal matches for the Wiking glacial till

is close to the value of 1.0 adopted by [Randolph \(1993\)](#) for similar analyses on 0.762mm open piles driven at Tilbrook Grange in stiff, low-plasticity, glacial Lowestoft till.

An example signal match is shown in Figure 23.

Table 11: Summary of equations and adopted parameters using models in IMPACT

	No.	Holocene & Glacial till	Chalk
Shaft resistance	$\tau = k_s w + c_s v \leq \tau_{stat}$		
Spring	$k_s = \frac{G}{\pi D}$		
Radiation dashpot	$C_s = \frac{G}{v_s} = \sqrt{G \rho_s}$	$G = G_1$	$G_{max} = (895 + 17.3z) \text{ (MPa)}$
Viscous effects	$\tau_{inter} = \tau_{stat} \left( 1 + \alpha_s \left( \frac{\Delta v}{v_0} \right)^{\beta_s} \right)$	$G_1 = 200 \sigma'_{vo} \text{ (MPa)}$	$G = G_1 = 0.2 G_{max} \text{ (MPa)}$
Base resistance	$Q = K_b w + C_b v \leq q_{b,stat}$	$\rho_s = 2.2 \text{ G/cm}^3$	$\rho_s = 2.2 \text{ G/cm}^3$
Spring	$K_b = \frac{4GR}{(1-v)}$	$\alpha_s = 1.15$	$\alpha_s = 1.1$
		$\beta_s = 0.2$	$\beta_s = 0.2$
		$v = 0.5$	$v = 0.5$
Radiation dashpot	$C_b = \frac{4R^2}{(1-v)} 0.8 \sqrt{G \rho_s}$		
Subsidiary mass	$m_0 = 0.16 \frac{4R^3 \rho_s}{(1-v)}$		

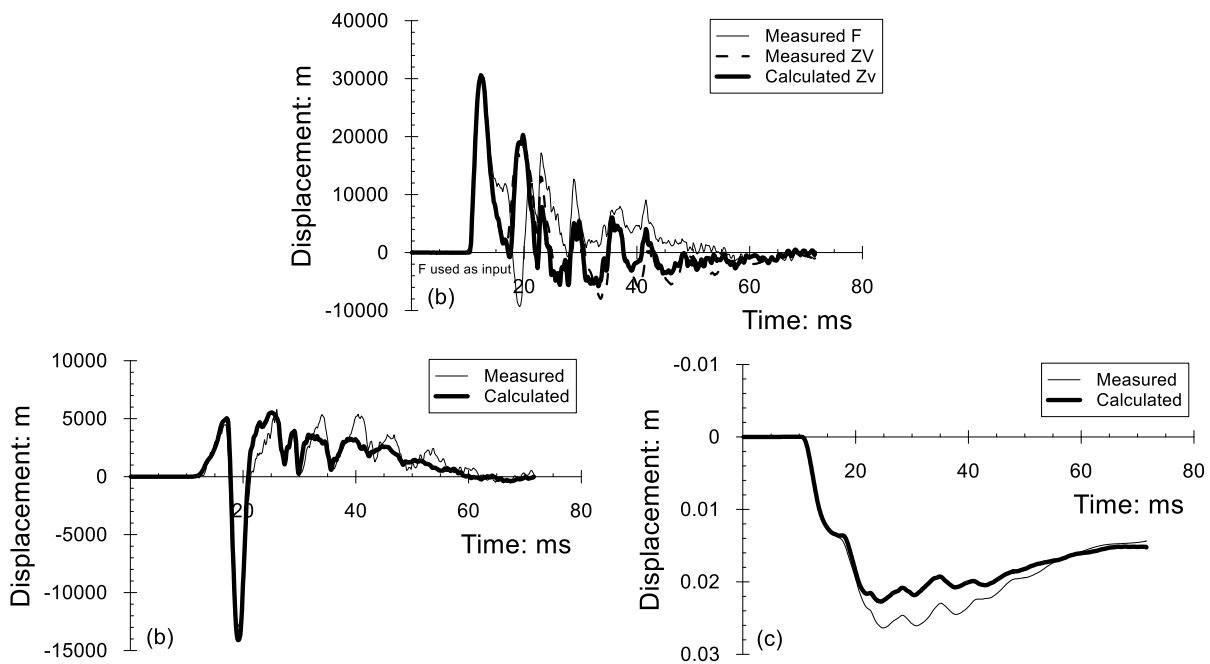


Figure 23: Example signal match from blow WK38-2\_DPT\_EOD: measured and calculated (a) force and velocity times impedance (b) upward travelling force (c) displacement